https://ntrs.nasa.gov/search.jsp?R=19700033818 2020-03-12T00:37:53+00:00Z

N 70 43134

54

CR 110895

LM CATHODE THRUSTER SYSTEM

FINAL REPORT SUPPLEMENT

18 JULY 1969 THROUGH 18 JULY 1970

CASE FILE COPY

CONTRACT JPL 952131

SEPTEMBER 1970

HUGHES

HUGHES AIRCRAFT COMPANY

RESEARCH LABORATORIES

MALIBU, CALIFORNIA

90265

HUGHES RESEARCH LABORATORIES
Malibu, California

a division of hughes aircraft company

LM CATHODE THRUSTER SYSTEM

Final Report Supplement
18 July 1969 through 18 July 1970
Contract No. JPL 952131

Performed for

Jet Propulsion Laboratory
California Institute of Technology

Sponsored by

National Aeronautics and Space Administration
Contract NAS 7-100 (Task Order No. RD-26)

15 October 1970

"This report contains information prepared by the Hughes Research Laboratories under JPL subcontract. Its content is not necessarily endorsed by the Jet Propulsion Laboratory, California Institute of Technology, or the National Aeronautics and Space Administration."

PROGRAM PARTICIPATION

Contributions by Members of the Technical Staff who participated in this program are acknowledged below.

PROGRAM MANAGEMENT	J. Hyman, Jr.
SYSTEM OPTIMIZATION AND TESTING	J. R. Bayless
DEVELOPMENT OF THE MERCURY FEED SUBASSEMBLY	D. E. Schnelker
THERMAL DESIGN AND ANALYSIS	J. R. Bayless, and J. W. Ward
POWER CONDITIONING DEVELOPMENT	J. Simpkins

ABSTRACT

A 20 cm LM cathode thruster system (designated LMT-20-II) has been developed for operation at beam currents I_B = 0.5 A to 1.0 A and a beam voltage $V_B \leq 2$ kV. At the maximum beam level, the total source energy per ion V_S = 315 eV/ion at a mass utilization efficiency η_m = 89%. Discharge chamber performance is essentially unchanged for operation at a reduced beam voltage V_B = 1 kV. The thruster employs a conventional thin-screen (0.076 cm thick), high-transparency (70%) ion-extraction system and an LM cathode which is thermally integrated with the thruster body. A mercury feed subassembly is joined to the thruster (within a common ground screen shroud) which consists of an electromagnetic pump, a liquid mercury flowmeter, and a high voltage isolator. The pump generates a pressure of 0.6 atm with a power of 2 W, and the flowmeter shows promise of a measurement accuracy of ±1%. At full rated power, the LM cathode operates at an equilibrium temperature $T_K < 200^{\circ}C$. With an overall mass of 6 kg (exclusive of propellant and reservoir), the LMT-20-II system operates with an over-all efficiency of η_T = 72% at a specific impulse $I_{sp, eff}$ = 4,040 sec or alternatively with η_T = 60% at $I_{sp, eff}$ = 2,710 sec. Thermal analysis indicates that cathode temperature can be reduced significantly by implementation of effective heat shielding on the inside walls of the discharge chamber.

TABLE OF CONTENTS

LIST OF ILLUSTRATIONS

SECTION I

INTRODUCTION

A electron-bombardment thruster system must demonstrate efficient and reliable operating capability within the constraints imposed by the mission. These constraints include the capability for electrically isolating an individual thruster from the propellant reservoir, and for interplanetary missions, the ability to throttle the ion beam over a two-to-one current range while maintaining high over-all efficiency. In previous experiments, the liquid mercury (LM) cathode thruster has demonstrated the ability to satisfy these requirements[1] and, therefore, serves as a viable element to fulfill future space propulsion requirements.

To facilitate detailed mission analysis and comparative evaluation of the LM cathode thruster with respect to other thruster types, a complete thruster system (including the subsystems for propellant feed, ion beam neutralization and power conditioning) must be built and its operating characteristics determined. As the first step toward construction of such a system, a 20 cm electron-bombardment thruster system (designated LMT-20-II) has been developed at the Hughes Research Laboratories (HRL). The system includes a 20 cm thermally-integrated LM cathode thruster and all of the components necessary for measurement and control of liquid mercury flow to the thruster. It is designed for operation at ion beam currents in the range $I_B = 0.5$ A to 1.0 A with an effective specific impulse $I_{sp,\ eff} \cong 4,000$ sec.

Prior to the current development, individual programs for research and development of the LM cathode, the thruster, and various elements of the liquid mercury feed system had been carried out as separately funded projects. Through coordinated guidance of the over-all program, these separate projects have produced the necessary

devices and technology which have now been employed in development of the LMT-20-II system. The feasibility of LM cathode thruster life in excess of 10^4 hours was demonstrated at Hughes Research Laboratories under Contract NAS 3-6262; a 20 cm thruster equipped with a circular LM cathode was successfully tested for an accumulated 4,000 hours. No erosion of the molybdenum cathode structure was evident following this test, and there was no degradation of cathode performance. In an extension of the same life test, an LM cathode neutralizer demonstrated a lifetime capability in excess of 500 hours. Development of high temperature LM cathodes began at HRL under Contract NASW-1404 after it became apparent from thermal analysis that combining thrusters in peripheral or clustered arrays places a constraint on the operation of any electron-bombardment ion thruster unless the temperature of the thruster shell can be allowed to exceed a value on the order of 200°C.

The demonstrated feasibility of system life in excess of 10^4 hours, combined with a demonstrated capability for operation of a high temperature LM cathode in an efficient thruster, prepared the way for the construction of a 30 cm thermally integrated thruster (designated the LMT-30-I thruster) under the first phase of the current contract. This thruster has now demonstrated efficient performance at a specific impulse $I_{sp,\ eff} = 4,100$ sec; a beam current $I_B = 1,400$ mA is produced at a beam voltage $V_B = 2$ kV with a source energy per ion $V_S = 270$ eV/ion* at a mass utilization efficiency $\eta_m = 90\%$. At this power level, the thermally integrated LM cathode achieves an equilibrium body temperature $T_K = 200°C$; it rejects discharge heat along a tapered aluminum endplate to the outer thruster shell, from which the heat is radiated to the walls of the vacuum chamber.

*V_S, the total source energy per ion, is the discharge energy per ion, because no heater, vaporizer, or keeper power is required with the LM cathode.

In a related contract effort (Contract NAS 7-539), the design of liquid-mercury feed systems was explored in detail. A number of unique components were built so that their operating characteristics could be established and the various systems could be properly evaluated. Two of these components, an electromagnetic pump and a high voltage isolator, were incorporated into a breadboard flow system which was operated under the first phase of the current contract for a demonstration of the proper operation of each of the components and of the mutual compatibility of all of the components of the system. The feed system consisted of (1) a gas-pressurized positive-expulsion mercury reservoir, (2) the liquid-mercury high voltage isolator, (3) the electromagnetic pump, (4) a single-capillary flow impedance, and (5) a high temperature LM cathode which was thermally integrated with the LMT-30-I thruster. Successful operation of this thruster with the breadboard liquid-mercury feed system led to the present development of the LMT-20-II thruster system.

SECTION II

SYSTEM CHARACTERISTICS

A. CONFIGURATION

Development of the LMT-20-II thruster system establishes a credible alternative to the hollow-cathode electron-bombardment thruster systems presently under consideration for various space applications. It has been designed such that integration can readily be accomplished into the SEPST III (Solar Electric Propulsion System Technology) system presently being developed at the Jet Propulsion Laboratory (JPL) of the California Institute of Technology.[2] In addition to being mechanically compatible with the SEPST III system, with only slight modification, the LM cathode system is capable of being electrically integrated with the power conditioning circuitry used with SEPST III hollow cathode thrusters. Circuitry which is particular only to the LM cathode system will be described as part of the LMT-20-II system.

As illustrated in Fig. 1, the LMT-20-II system requires only electrical inputs and a supply of liquid mercury for its operation. The thruster and mercury feed subassembly are characteristically enclosed within a single ground-screen shroud. The mercury feed subassembly which supplies liquid mercury to the long-life LM cathode, consists (in order of flow sequence) of a high voltage isolator, an electromagnetic (EM) pump, a mercury flowmeter, and a single-capillary flow impedance. This subassembly facilitates precise measurement and control of the propellant flow rate while providing electrical isolation between the thruster and the mercury reservoir. The total weight of the LMT-20-II system, including the thruster and the ion-extraction system, the mercury feed subassembly, and the ground-screen shroud

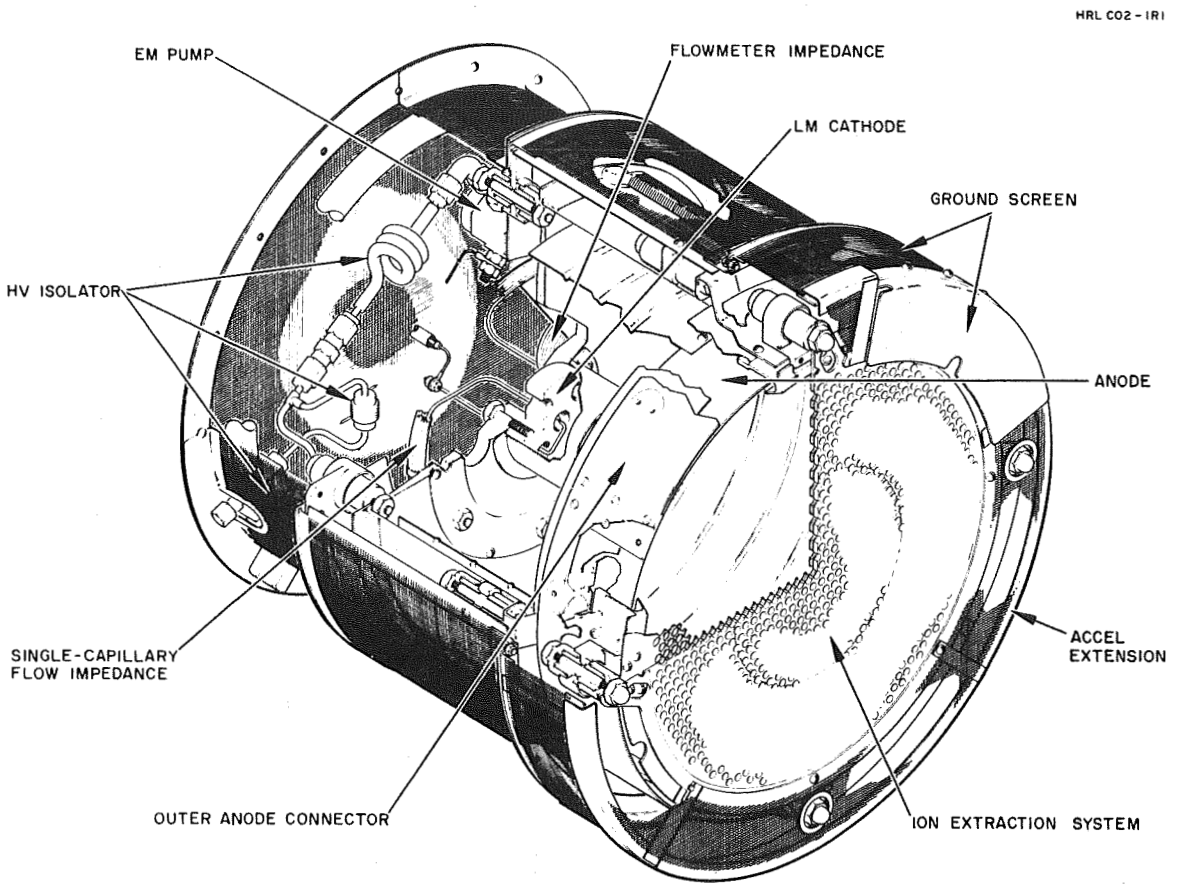

Fig. 1. Isometric drawing of the 20 cm LM cathode thruster system (LMT-20-II).

is approximately 6 kg. The present work has not included development of a discharge igniter or LM cathode neutralizer, although provision has been made for incorporating both of these elements; laboratory versions of a high voltage spark igniter[3] and of an LM cathode neutralizer[4] have both been demonstrated at HRL under earlier efforts.

B. SYSTEM CONTROL

To optimally achieve the goals of a specific propulsion mission, the elements of the LMT-20-II system must be combined with logic and control circuitry to maintain efficient operation and to regulate and control the thrust schedule as determined by mission requirements. Though no hardware has yet been built for automatic control of the LMT-20-II system, a general control scheme has been developed. A schematic diagram is presented in Fig. 2 which shows the manner by which the elements of the thruster system are operated by the power-conditioning and control circuitry. By reliance in this system on direct measurement and control over the mercury flow rate, a significant advance is achieved in the direction of stable and accurate control over thruster operation.

The logic of the control scheme for the LM cathode thruster system can best be explained by picturing the cathode current as exercising primary control over ion beam current. This is a sensitive and single-valued relationship, because the beam current I_B increases almost linearly with discharge current I_K at a constant value of propellant utilization efficiency. By means of a second control loop, the propellant utilization efficiency η_m is held at the desired value by control of propellant flow rate. The flow rate which is measured by the flowmeter is expressed as an equivalent electrical current I_{Hg} which when multiplied by the required value of mass utilization efficiency ($0 < \eta_m < 1$) is compared with the required beam current to produce an

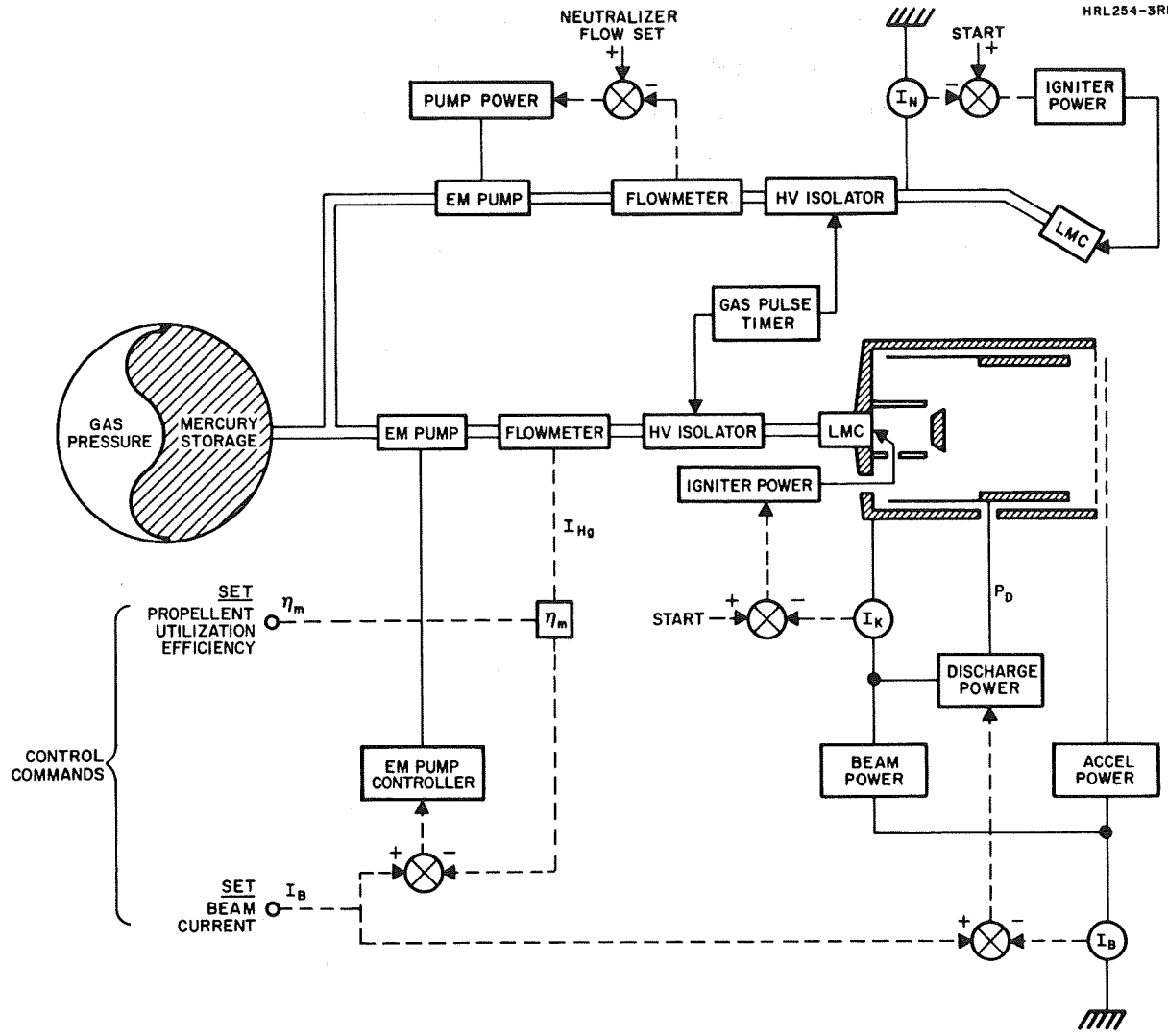

Fig. 2. Control logic for LMT-20-II thruster system.

error signal. If the product $I_{Hg}\ \eta_m$ equals I_B, no error signal is generated to drive the EM pump power controller. Small differences from this equality, however, can be used to generate relatively large signals to drive the EM pump so that a near equality will always be obtained. High feedback gain is possible in the flow control loop, because this loop is absolutely stable by virtue of the viscous damping forces derived from mercury flow through the single-capillary impedance.

The control scheme shown in Fig. 2 enjoys an added measure of stability beyond that of the scheme now employed for control of the SEPST III hollow-cathode thruster system. In that system, the beam current I_B is controlled by varying the mercury flow rate through the main propellant vaporizer. The desired value of propellant utilization efficiency η_m is obtained only indirectly by reliance on a functional relationship between beam current I_B and cathode discharge current I_K. Unfortunately, the beam-current control relationship is not entirely single-valued for operation of highly optimized thruster systems (above a certain maximum value, the beam current is reduced by increases in propellant flow rate), and system control is lost if thruster operation occurs beyond prescribed limits.[2] Though definite and repeatable functional relationships between beam current, discharge current, and propellant utilization efficiency also exist with the LM cathode thruster, reliance in the LMT-20-II system on the direct measurement and control of the liquid mercury flow rate provides sufficient information for unambiguous control over all relevant parameters.

C. SYSTEM EFFICIENCY

Data obtained from operation of the LMT-20-II system (see Section III for details of thruster performance and Section IV for performance details concerning the mercury feed subassembly) provide a basis for comparative evaluation with other electron bombardment

thruster types. The total efficiency of the over-all thruster system is evaluated in Table I for operation at $I_B = 1.0$ A; no separate tabulation is listed for operation at reduced beam current, because differences in performance are small and the details of these differences are not felt to be significant. The over-all efficiency reaches a maximum value $\eta_T = 72\%$ for operation at the design impulse $I_{sp,\ eff} = 4,040$ sec and decreases to a value of $\eta_T = 60\%$ for operation at a specific impulse $I_{sp,\ eff} = 2,710$ sec.

TABLE I

Efficiency of the LMT-20-II Thruster System

Effective Specific Impulse, $I_{sp,eff}$	4,040 sec	2,710 sec
Beam Voltage, V_B	2 kV	1 kV
Beam Current, I_B	1 A	1 A
Source Energy Per Ion, V_S	315 eV/ion	315 eV/ion
Beam Mass Utilization Efficiency, η_m	89%	89%
Neutralizer Coupling Voltage, * V_{N-C}	30 V	30 V
Neutralizer Mass flow fraction, * $\eta_{m,N}$	3%	3%
Accel Interception Current, I_{Ac}	6 mA	25 mA
Thruster Power, $P_B = I_B V_B$	2,000.0 W	1,000.0 W
Discharge Power, $P_S = I_B V_S$	315.0 W	315.0 W
Neutralizer Power, $P_N = I_B V_{N-C}$	30.0 W	30.0 W
Accel Electrode Power, $P_{Ac} = I_{Ag} (V_B - V_{Ac})$	24.0 W	75.0 W
Isolator Power, + P_{Is}	0.7 W	0.7 W
EM Pump Power, + P_{EM}	1.0 W	1.0 W
Flowmeter Power, + P_F	1.0 W	1.0 W
Total System Power, ** P_T	2,371.7 W	1,422.7 W
Total System Power Efficiency, $\eta_{P,T} = P_B/P_T$	84%	70%
Total System Mass Utilization Efficiency, $\eta_{m,T} \approx \eta_m - \eta_{m,N}$	86%	86%
Total Thruster System Efficiency, $\eta_T = \eta_{P,T} \cdot \eta_{m,T}$	72%	60%

*No neutralizer was operated with the LMT-20-II system, but neutralizer losses have been estimated from data obtained in earlier operation of the LMT-30-I system.

**This value has been determined assuming the use of permanent magnets. During experimentation, bar electromagnets were used to achieve greater operating flexibility. Approximately 16 W was consumed by these magnets.

+Power requirements for the mercury feed subassembly are listed in Table II of Section III.

SECTION III

PERFORMANCE OF THE LMT-20-II SYSTEM

The LMT-20-II thruster (shown in Fig. 3) has demonstrated satisfactory performance throughout the design range of beam current from I_B = 0.5 A to 1.0 A when operated together with the mercury feed subassembly. At the maximum beam level, stable operation was demonstrated at a total source energy per ion V_S = 280 eV/ion with a mass utilization efficiency η_m = 80%, and also at V_S = 315 eV/ion with η_m = 89%. Throughout the design range, ion beam interception by the accel electrode was less than 1% for operation at a beam voltage V_B = 2 kV. Performance of the thruster system was essentially unchanged for operation at beam voltages as low as V_B = 1 kV (at this voltage, the effective specific impulse is $I_{sp,\ eff}$ = 2,710 sec at η_m = 89%) except for an increase in ion beam interception by the accel electrode to a value in excess of 1% for operation below V_B = 1.5 kV. A maximum interception of 2-1/2% was observed at a beam current I_B = 1.0 A and a beam voltage V_B = 1 kV.

A. DISCHARGE CHAMBER PERFORMANCE

Discharge chamber performance for operation of the LMT-20-II system is shown in Fig. 4. For thruster operation with a mass utilization efficiency η_m = 80%, the total source energy per ion is relatively independent of beam current over the design range from I_B = 0.5 to 1.0 A. This uniformity in operation is interpreted as indicating the general suitability of the LM cathode thruster system for throttling of the beam current as required to optimally achieve mission objectives, a capability demonstrated in the operation of the nonthermally integrated LMT-20-I thruster which was reported earlier.[1] It should be noted that

M 6936

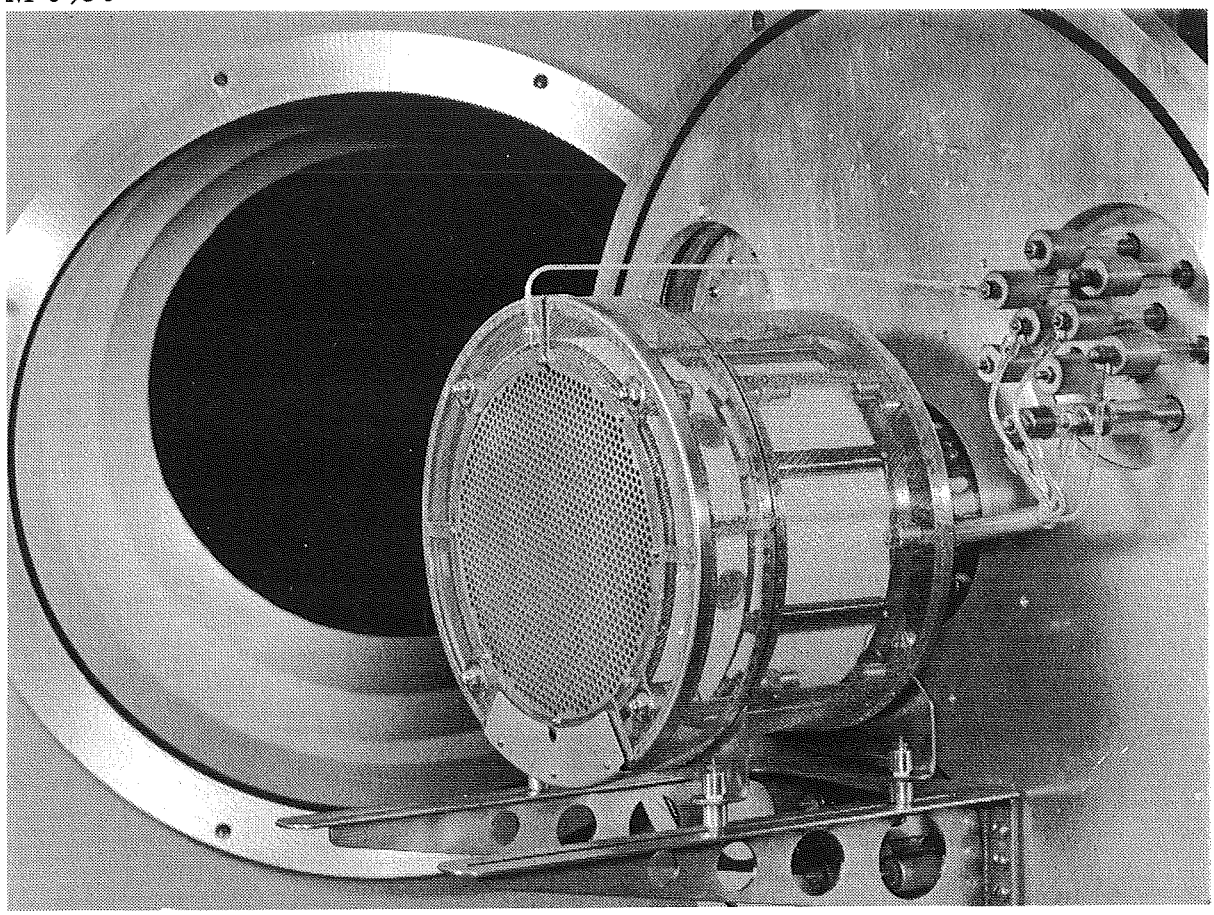

Fig. 3. The LMT-20-II thruster shown mounted on the vacuum chamber endplate.

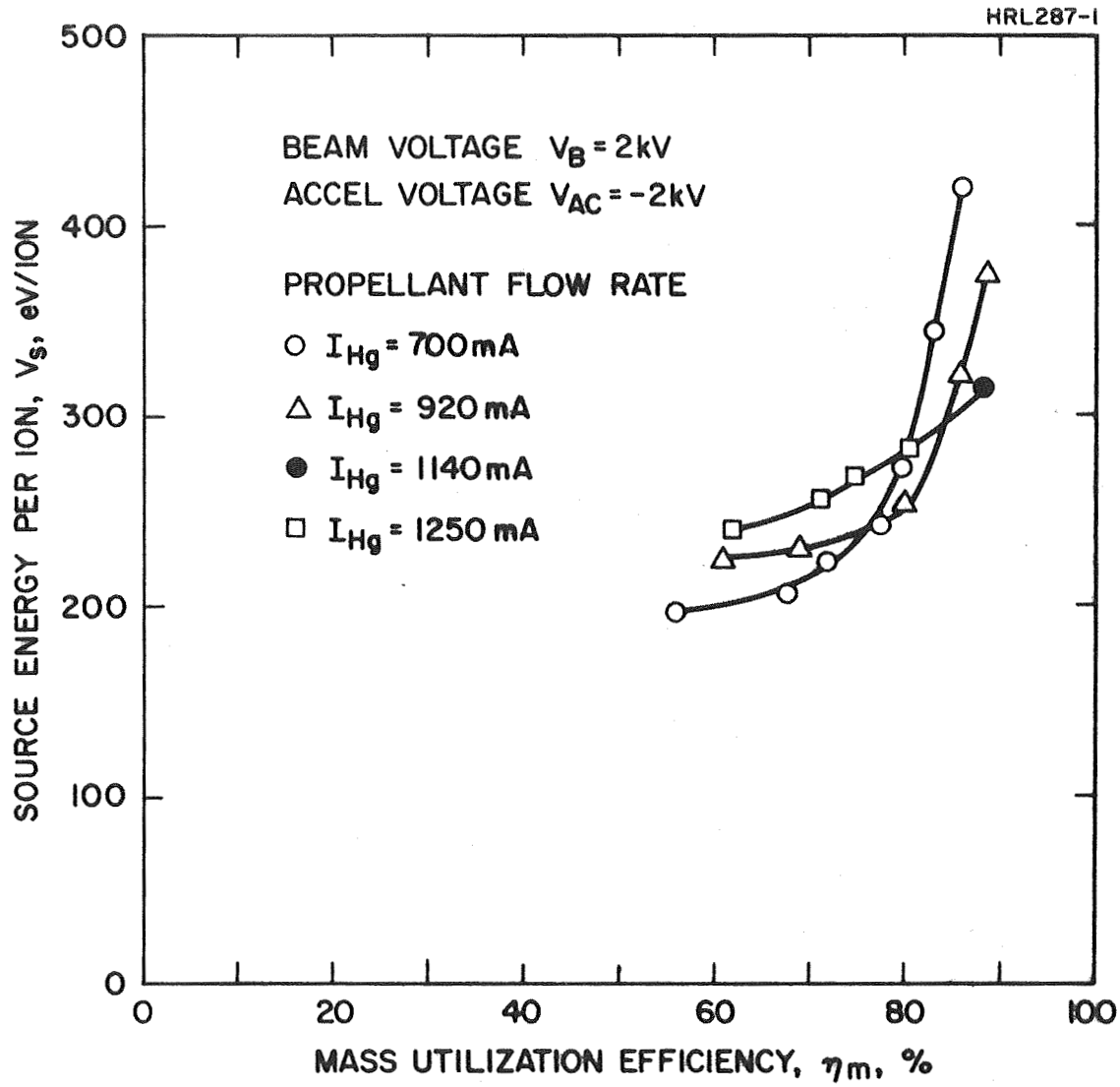

Fig. 4. Discharge chamber performance of the LMT-20-II system.

the data of Fig. 4 are only typical of system performance and not representative of the ultimate performance which might be achieved after exhaustive optimization.

B. ION-EXTRACTION CHARACTERISTICS

Two sets of conventional ion-extraction electrodes have been tested with the LMT-20-II system. The accel electrode of one set has a uniform thickness of 0.254 cm, while that of the second set is tapered to a thickness of 0.127 cm at the outer diameter. The accel electrode is supported by four insulating supports on a bolt circle of 24.4 cm. The screen electrode has a thickness of 0.076 cm and the 0.475 cm diameter ion beam apertures are oriented in a hexagonal close packed array with a distance between hole centers of 0.535 cm. Similar performance is demonstrated in operation of the LMT-20-II system with either set, though a reduction in mass from 610 to 444 g is achieved by use of the tapered design. The data reported in this paper were obtained for operation with the accel electrode of uniform thickness.

Though operation at reduced values of specific impulse has negligible effect on discharge chamber performance, the increase of ion beam interception by the accel electrode is clearly evident from the data of Fig. 5. While generally less than 1% of the total beam current for beam voltages greater than V_B = 1.6 kV, accel interception rises steeply for lower beam voltages to a value of about 2-1/2% at a beam voltage V_B = 1 kV.

C. THERMAL CHARACTERISTICS

The LM cathode dissipates all discharge heat by conduction to and radiation from the thruster shell. Over the range of beam current, temperatures of the major thruster elements were measured. Equilibrium values are shown in Fig. 6 as a function of total discharge power.

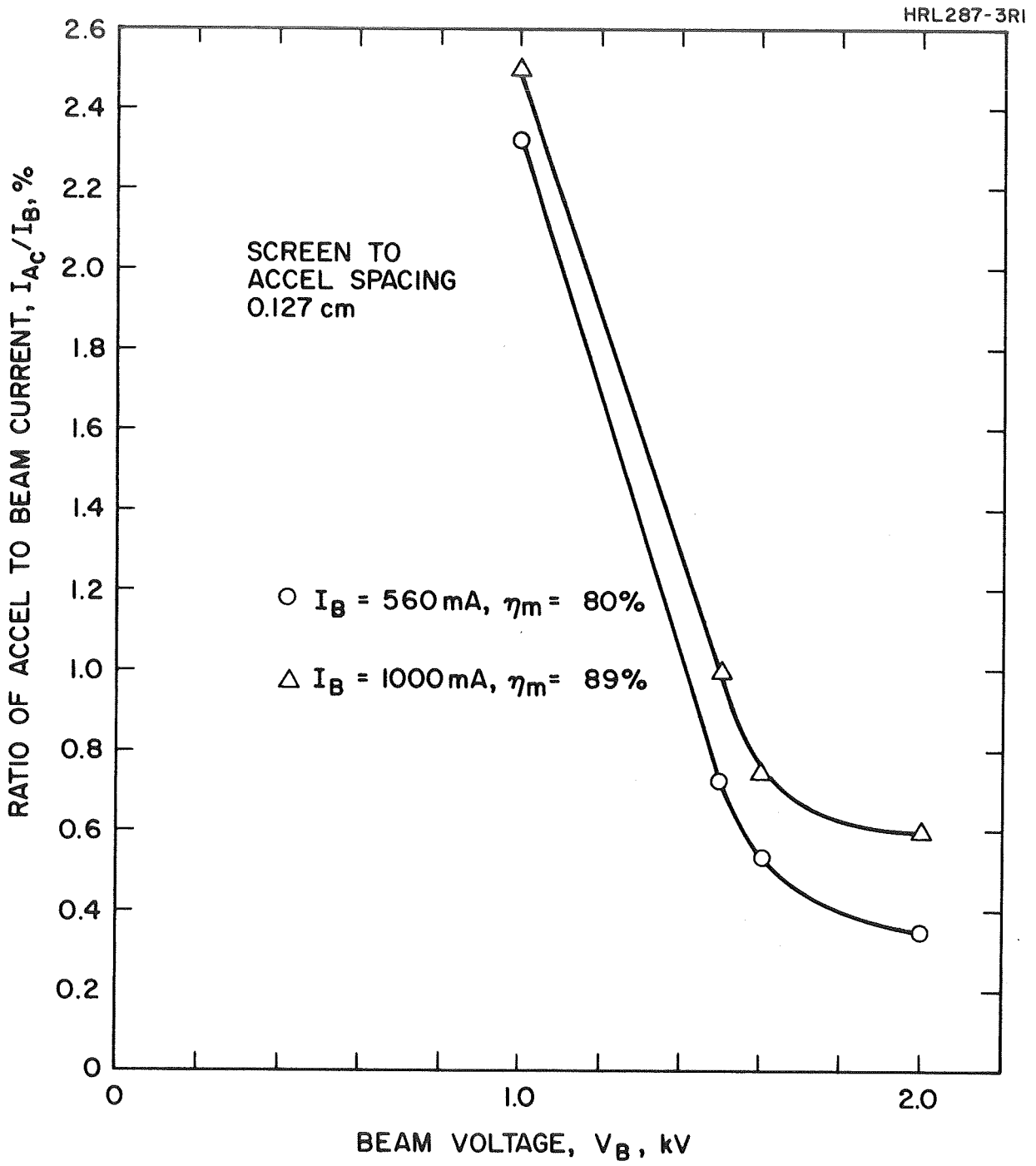

Fig. 5. Ion beam interception by the accel electrode as a function of beam voltage.

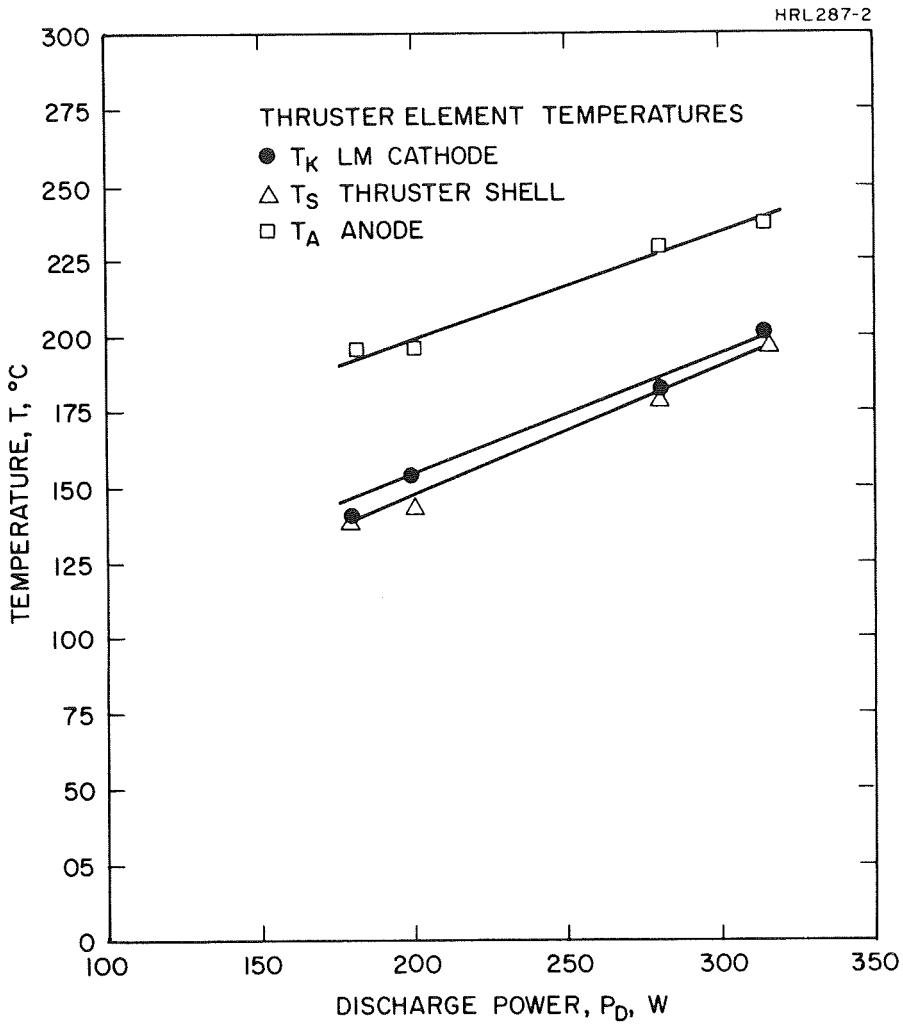

Fig. 6. Equilibrium temperatures of thruster elements as a function of discharge power.

Though the temperature of the LM cathode lies within the limits for efficient operation, the measured values are significantly higher than were anticipated from analysis of the thermal design (see Section V). Whereas cathode temperature reaches a value $T_K = 185^{\circ}C$ for a discharge of 280 W, analysis of the LMT-20-II system had predicted operation at a temperature of $T_K = 121^{\circ}C$.

The higher value of measured cathode temperature indicates that the heat shielding which was employed for operation of the LMT-20-II thruster has not performed effectively. While the thermal characteristics of the LMT-20-II thruster system are entirely satisfactory for operation of a single thruster, effective heat shielding is essential if several identical thrusters must be operated at full power simultaneously in closely clustered arrays with heat rejection solely by radiation from the thruster shell.* In order to minimize the cathode temperature in the LMT-20-II design, the outer surface of the thruster body was covered with high emissivity ($\epsilon = 0.85$) paint. Eleven heat shields, consisting of 6061 aluminum foil, covered both the inside surface of the thruster endplate and the upstream two-thirds of the anode extension. The heat shielding which covers the anode extension is visible in the photograph of the LMT-20-II thruster, as shown in Fig. 7.

The higher value of measured cathode temperature is best explained by the assumption that the separation between the multiple aluminum heat shields had completely collapsed during thruster operation such that the shields were entirely ineffective in their ability to reduce heat flow from the discharge chamber into the thruster shell.

*No heat shielding is required if heat conduction is permitted between the thruster and the spacecraft, or if a separate radiator is provided for control of cathode temperature, or if the system is operated at reduced power.

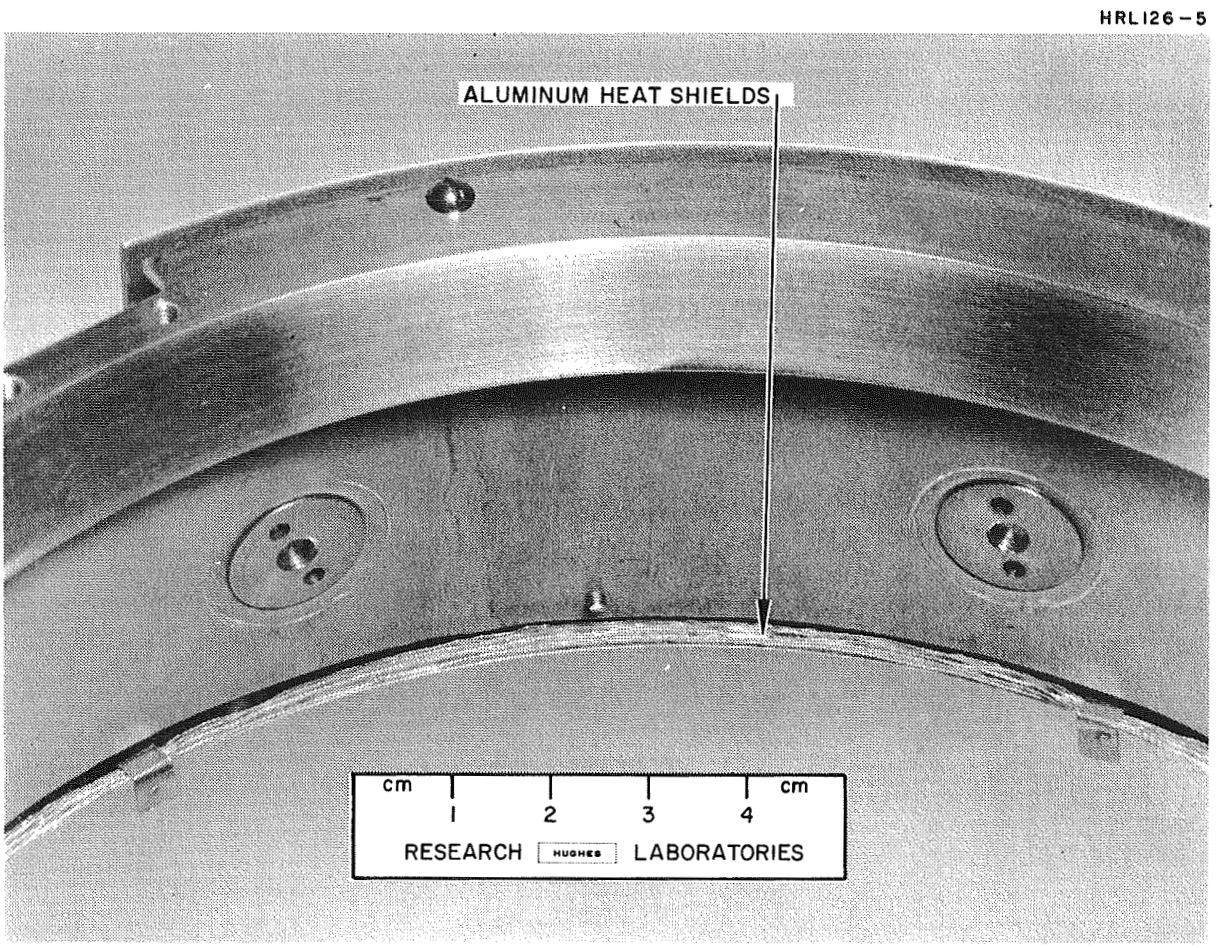

Fig. 7. The LMT-20-II thruster showing the heat shielding which covers the anode extension.

By adopting alternate techniques for installation of heat shields in future operation of the LMT-20-II system, detailed thermal analysis has indicated that cathode operating temperatures will be decreased to the extent that simultaneous operation of multiple thrusters will be possible in closely clustered arrays with heat rejected by radiation from the thruster shell alone.

D. MERCURY FEED SUBASSEMBLY

Operation of the LMT-20-II thruster system was facilitated by the use of flight-type LM cathode K-54 in conjunction with the mercury feed subassembly shown in Fig. 8. With its single-capillary flow impedance, LM cathode K-54 operated stably for hours at a time without arc extinction. In contrast to the operation of earlier LM cathodes which used porous tungsten impedances to regulate mercury flow[1,3], data acquisition was expedited considerably by the linear and repeatable flow characteristics of the single-capillary flow impedance.* With the thruster operating at a voltage V_B = 2 kV, the mercury reservoir was held at ground potential with high voltage isolation provided by a device which injects hydrogen bubbles into an insulated section of the propellant flow line to interrupt electrical continuity through the liquid mercury.[5] Once every half hour, an all solid-state power-conditioning subassembly supplies 2.8 min duration pulses of 7 W electrical power to activate the hydrogen-bubble injection element.

Both the EM pump and the liquid-mercury flowmeter were incorporated into the LMT-20-II system though no parametric measurements

*Data acquisition is hampered also by thermal feedback from the cathode when a porous tungsten impedance is placed close to the cathode (which is the practice in LM cathodes and for the porous tungsten vaporizer of thermally integrated hollow cathodes). This feedback establishes an interaction between the discharge current and the propellant flow rate.

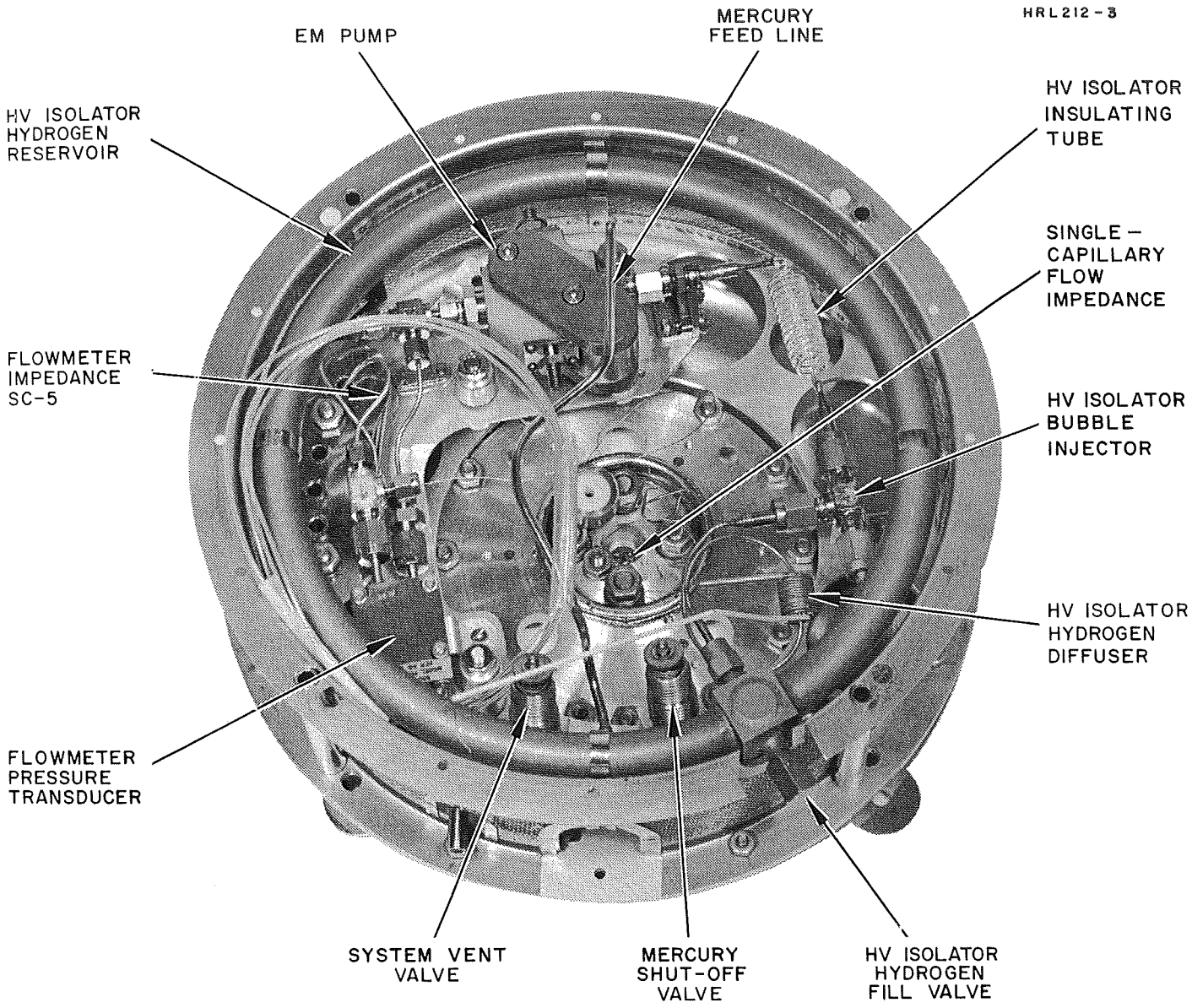

Fig. 8. Photograph of the LMT-20-II mercury feed subassembly.

of the operation of these elements were recorded in conjunction with thruster operation. Detailed performance characteristics were obtained, however, in separate component tests which were carried out prior to assembly of the LMT-20-II system. While the description of these tests is deferred to Section V, a tabulation of the power requirements for each element of the LMT-20-II mercury feed subassembly is presented in the following Table II.

TABLE II

Power Requirements for the LMT-20-II
Mercury Feed Subassembly

Element	Peak Power, W	Average Power, W
HV Isolator	7.0	0.7
EM Pump	2.0	1.0
Flowmeter	1.0	1.0
		2.7 Total

SECTION IV

DESIGN OF THE LMT-20-II THRUSTER SYSTEM

The LMT-20-II system was designed to operate at beam currents in the range I_B = 0.5 A to 1.0 A and to dissipate all heat resulting from discharge losses by radiation. The discharge chamber configuration was modified only slightly from that of the LMT-20-I thruster developed during the earlier phase of this contract,[1] which was operated at a lower beam current with an externally cooled LM cathode. The thermal design and the thin screen, high transparency ion extraction system are similar to those in use with the LMT-30-I thruster developed at the same time as the LMT-20-I thruster.

Although the thruster and its liquid-mercury feed system are characteristically enclosed within the single ground-screen shroud shown in Fig. 1, provision was made in the design to allow the two subsystems to operate as separate units. This has permitted the separate development of the feed system to proceed simultaneously with the optimization of the thruster prior to integration of the thruster system.* A screened enclosure extends the accel electrode and completes the enclosure formed by the ground screen. Although no neutralizer development was carried out under this contract, provision was made for mounting an LM cathode neutralizer over a sheet metal extension of the ground screen which covers one quadrant of the accel extension screen. Table III lists the mass of each component of the

*The LMT-20-II thruster was shown in Fig. 3 in the configuration of the first experimental operation which was implemented by use of single-capillary fed LM cathode K-51 and a piston-driven liquid mercury supply, while the mercury feed subassembly was checked out by bell jar testing in the configuration shown in Fig. 9.

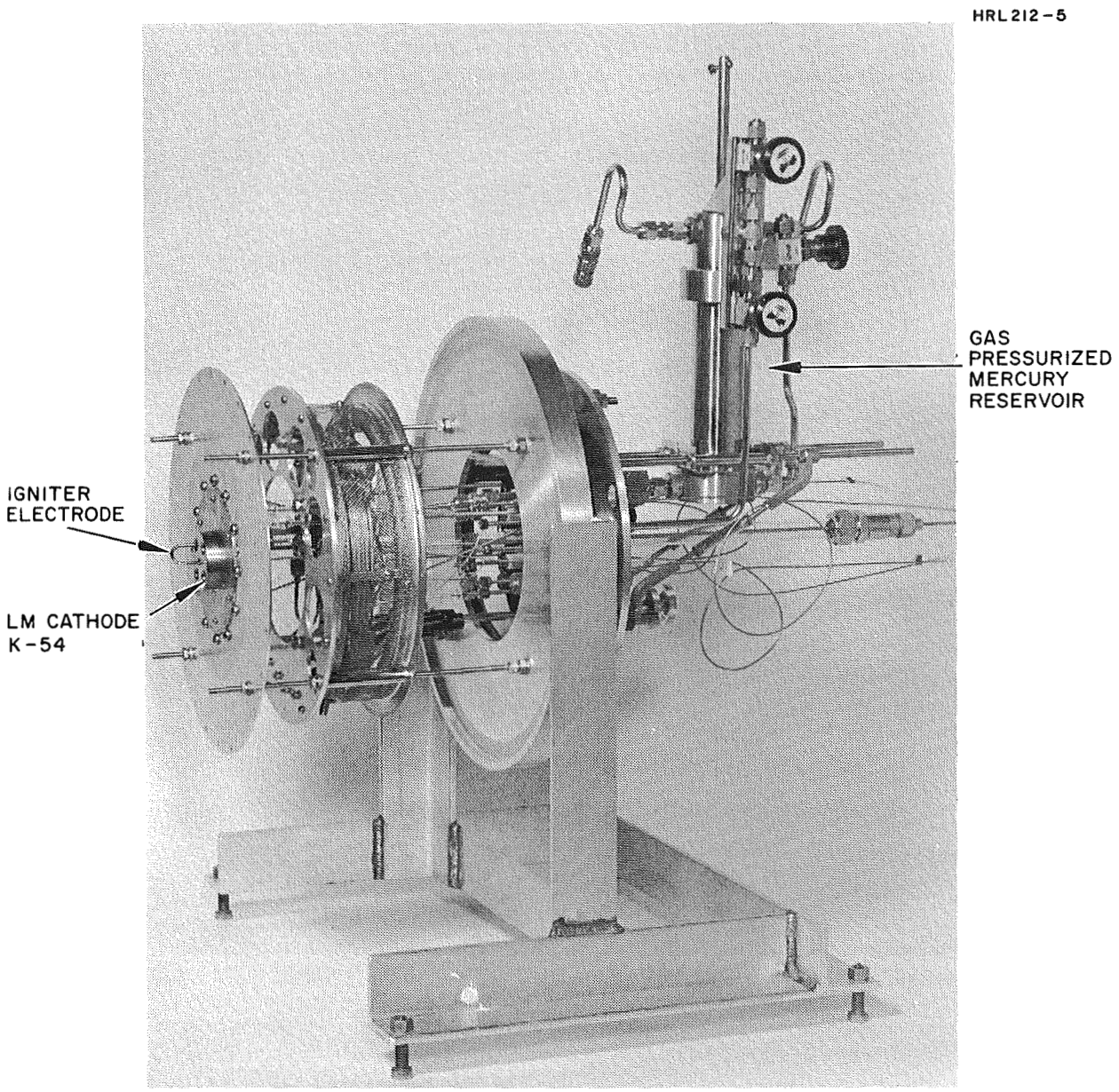

Fig. 9. LM cathode K-54 and the LMT-20-II mercury feed subassembly mounted for bell jar testing.

TABLE III

Component Masses of the LMT-20-II Thruster System

Component	Part No.	Quantity per Assembly	Weight of Assembly, kg
Thruster			
Thruster Shell Assembly	839924	1	0.499
Band, Anode Feedthrough	839925	1	0.046
Anode, Upstream	839926	1	0.132
Anode, Downstream	839927	1	0.076
Outer Anode Connector	839928	1	0.087
Ceramic Spacer	839929	8	0.012
Accel. Electrode	839930	1	0.444
Screen Electrode	839946	1	0.155
Stud	839931	4	0.022
Shield Insulator	839932	8	0.014
Bracket, Insulator, Center	839933	4	0.039
Support, Insulator, Accel.	839934	4	0.062
Support, Magnet, Upstream	839937	1	0.125
Splice Plate Assembly	839938	1	0.005
Pole Piece, Outer, Upstream	839940	2	0.141
Pole Piece, Inner, Upstream	839941	2	0.044
Pole Piece, Upstream Cover	839942	1	0.057
Screen Pole Piece	839947	1	0.349
Magnet With Windings	839948	8	0.884
Nut & Screw-Mtg. Anode Sink	1024015	16	0.066
Ceramic Insulator, Feedthrough	1024016	8	0.088
Feedthrough, Anode	1024017	8	0.048
Screw, Shouldered	1024018	8	0.003
Removable Endplate	1024128	1	0.183
LM Cathode K-54		1	0.131
Heat Shields		10	0.309
Total			4.021
Feed System			
Plate, Feed System Support	1024127	1	0.036
Mount, Flowmeter	1024129	1	0.002
Mount - EM Pump	1024130	1	0.005
Retaining Nut, Isolator Connector	1029132	1	0.005
Connector Isolator	1029134	2	0.001
Hydrogen Reservoir	1024145	1	0.218
Isolator		1	0.089
EM Pump		1	0.301
Flowmeter		1	0.108
"Swagelok" Couplings		6	0.112
Plate, Feed System	1024059	1	0.111
Capillary Impedance		5 meters	0.040
Total			1.018
Ground-Screen Shroud			
Accel. Extension	1024019	1	0.094
Ground Screen, Center	1024020	1	0.240
Ground Screen, Optics Insulator	1024021	1	0.130
Ground Screen, Neutralizer Cover	1024022	1	0.013
Ground Screen, End Cover	1024024	1	0.096
Ground Screen, Feed System	1024114	1	0.197
Stud	839931	8	0.050
Shield Insulator	839932	16	0.028
Ceramic Spacer	839929	16	0.024
Support, Insulator, Center	839935	4	0.012
Support, Insulator, Upstream	839936	4	0.024
Total			0.908
Total Weight of Assembly			5.947

thruster system. The total mass (including the thruster and ion-extraction system, the liquid-mercury feed system, and the ground-screen shroud) is approximately 6 kg.

A. THRUSTER DESIGN

1. Discharge Chamber

Discharge chamber design of the LMT-20-II thruster depended heavily on the configuration of the LMT-20-I thruster. During the initial phase of Contract JPL 952131,[1] this thruster was optimized for operation at a beam current I_B = 600 mA. At a beam voltage V_B = 2 kV, the total source energy per ion was V_S = 280 eV/ion at a mass utilization efficiency η_m = 80%. As an initial task of the current effort, the LMT-20-I thruster was reoptimized for operation at beam currents in the range of 0.5 A to 1 A. Reoptimization of the discharge chamber involved modifications in the geometry of the baffle and of the cathode-cup pole piece.

Both at HRL and elsewhere,[6] the tendency has been noted for discharge voltage to decrease as propellant flow through the cathode increases, where the geometrical parameters of the discharge chamber are held constant. Reduction of discharge voltage can result in degradation of discharge chamber performance. With a fixed geometry of the openings which connect the cathode-cup region with the main discharge chamber, increased propellant flow through the cathode of an LM cathode thruster results in increased particle density within the cup region as well as within those openings, so that (without reference to a specific mechanism) a degradation of performance has resulted from this density increase.

A technique for extension of the efficient operation of an LM cathode thruster to a higher value of beam current has previously been established at HRL in the development of the LMT-30-I thruster.[1] To

permit operation of the 30 cm thruster at higher values of beam current, a cathode-cup pole piece was used which employed 36 holes in its cylindrical side wall; these holes were covered by a 20 wire/cm stainless steel screen. Selection of the size and number of these holes permitted the independent adjustment of the flow conductances (between cup region and main discharge chamber) for electrons on the one hand and for the propellant atoms on the other. The electrons pass predominantly through the gap between cup and baffle, while the propellant escapes predominantly through the screened holes. With this modification, it had been possible to adjust flow conditions so as to achieve the optimum values of plasma density within the cup and its openings while operating the thruster in the required range of propellant flow rate and discharge current.

Using the same technique, it has been possible to achieve efficient operation of the 20 cm thruster at beam currents up to I_B = 1 A. The required modifications were carried out initially in the LMT-20-I configuration. This thruster was equipped at an early stage of the program with a thin-screen high-transparency ion-extraction system similar to the one used with the LMT-20-II thruster. After a program of optimization, the discharge chamber configuration found to yield optimum performance with the LMT-20-I thruster was used as an initial configuration for the LMT-20-II thruster. Details of the LMT-20-II discharge chamber are shown in Fig. 10 in the configuration for which performance data have been reported. Electrons and neutral mercury vapor are supplied to the thruster discharge by single-capillary LM cathode K-54. Uniform propellant distribution within the discharge chamber is promoted by 24 screened propellant-diversion ports (each 0.79 cm in diameter) located in the cathode-cup pole piece. The cup itself is 4.2 cm long with an outside diameter of 5 cm and a wall thickness of 0.051 cm. Electron flow into the discharge chamber is regulated by an electron flow baffle which has a conical edge. The axial position of the baffle was left variable in order to facilitate performance optimization.

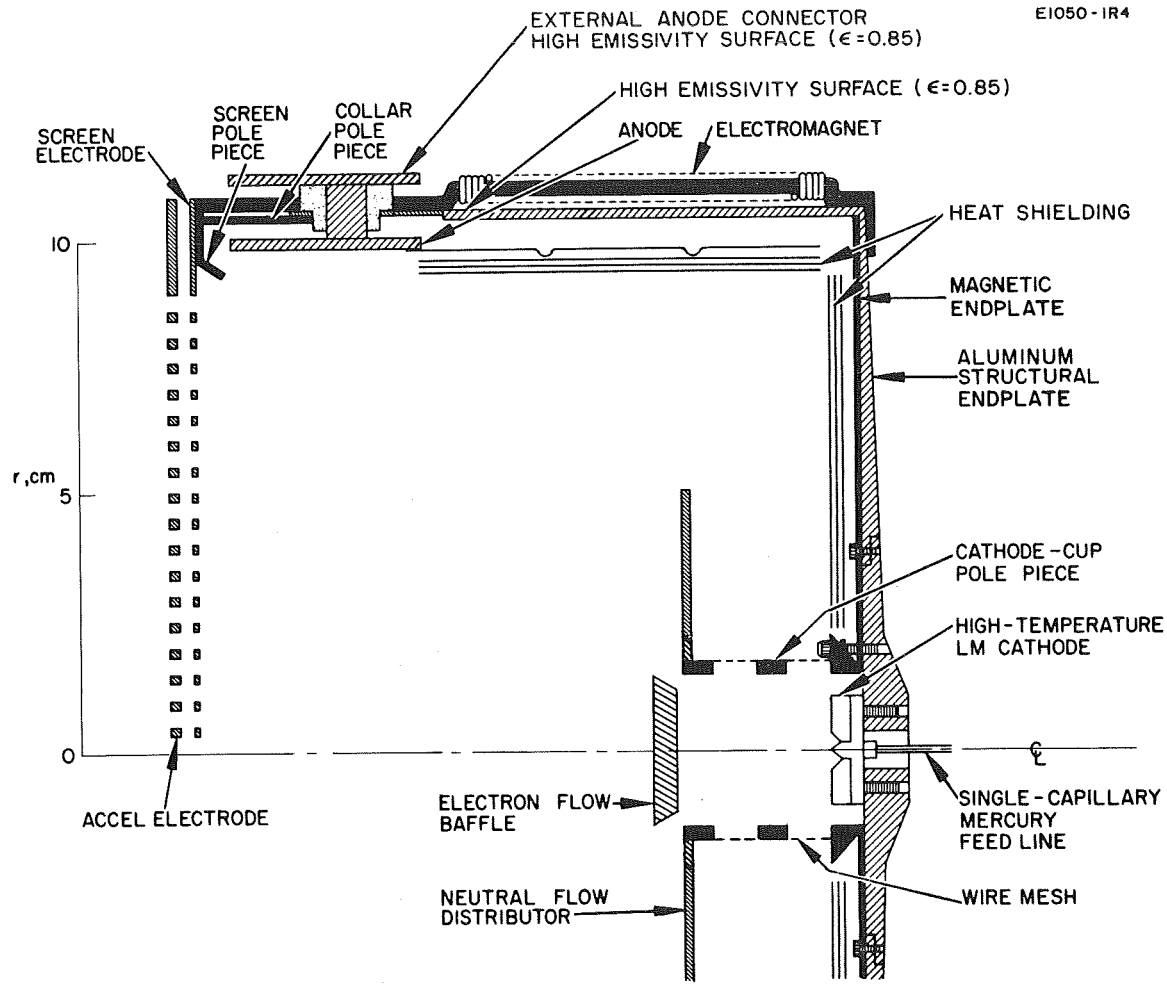

Fig. 10. Schematic cross-section of the LMT-20-II discharge chamber.

The anode diameter of the LMT-20-II thruster is 20 cm, and the length of the discharge chamber from screen to endplate is 16.5 cm. The anode is segmented into two parts: a thermally conductive aluminum portion in the region closest to the screen electrode and a thin, nonconductive, stainless steel portion comprising the upstream two-thirds of the anode.

2. Thermal Design

The thermally conductive portion of the anode is attached to an external connector by a series of leadthroughs consisting of short aluminum rods which pass through insulating ceramic sleeves. These leadthroughs serve the dual purpose of connecting the anode to the external electrical circuits, and conducting to the external connector the discharge heat which is delivered to the anode. The anode heat (which constitutes the major fraction of the total source power) is dissipated by radiation to space through the apertures of the ion-extraction system and from the outer surface of the external anode connector which is covered with a high-emissivity ($\epsilon = 0.85$) coating to increase the thermal radiation. This coating is applied as a water solution of a mixture of potassium silicate and titanium dioxide in a dry weight ratio of one to four.

Discharge heat, which is generated at the cathode, passes from the molybdenum body of the LM cathode directly into the aluminum enplate of the thruster. This endplate is tapered in order to achieve low weight while maintaining high thermal conductivity to the cylindrical thruster shell with is also covered with the high-emissivity coating.

Downstream of this position, the thruster shell consists of a thin band of stainless steel which reduces conductive coupling between the cathode and anode thermal circuits. In an attempt to further decouple the two thermal circuits, heat shielding (consisting of 11 layers of 6061 aluminum foil) was placed over the downstream surface

of the discharge chamber endplate and over the upstream two-thirds of the inner surface of the anode.

The thickness of the aluminum structure was chosen as a compromise between the opposing requirements for good thermal conduction between the cathode and lateral thruster wall and for light weight. As in the LM-30-I thruster, the cylindrical wall is fabricated to a thickness of 0.150 cm. The aluminum endplate is 0.150 cm thick where it joins with the cylindrical aluminum wall, and increases in thickness inversely with the radius up to the point of attachment of the LM cathode.

Aluminum was chosen as the major structural material because of its combined properties of light weight and high thermal conductivity, which together have resulted in the design of a lightweight thermally integrated thruster. Initially the decision was made to employ aluminum for fabrication of the LMT-30-I thruster, with the understanding that under certain conditions in air mercury is known to attack aluminum in a highly destructive manner. The literature[7] indicates, however, that alloys of aluminum with low silicon content have shown good resistance to such attack. Experience at HRL led to the choice of low silicon content 6061 aluminum alloy as the major structural material for thruster fabrication. To date, no mercury attack has been observed in the LMT-30-I or the LMT-20-II thrusters.

3. Ion-Extraction System

Design of the LMT-20-II ion-extraction system was based primarily on the same criteria which determined the design of the LMT-30-I system,[1] which has performed satisfactorily throughout its 200 hours of accumulated operation. The hole pattern was modified only slightly from that of the 30 cm system and is now identical with that used by Masek and Pawlik at JPL[2]. The plate thickness, hole pattern, and shape of the ion-extraction apertures are described in Table IV.

TABLE IV

Design Specifications for the LMT-20-II Ion-Extraction System

Electrode	Material	Thickness, cm	Hole Diameter, cm	Distance Between Hole Centers, cm	Hole Shape
Screen	Molybdenum	0.076	0.475	0.535	Circular
Accel	Molybdenum	0.254	0.365	0.535	Circular

Two sets of ion-extraction electrodes have been fabricated. The accel electrode of one set has a uniform thickness of 0.254 cm, while that of the second set is tapered to a thickness of 0.127 cm at the outer diameter. The accel electrode is supported by four insulating supports on a bolt circle of 24.4 cm, which is compatible with that used at JPL.

4. Magnetic Field Configuration

The thruster magnetic field is generated by eight electromagnets spaced uniformly around the exterior of the discharge chamber. This number of electromagnets was chosen as being few enough to provide sufficient space for mounting of other thruster components and yet numerous enough to generate a magnetic field of uniform azimuth within the discharge chamber. The screen pole piece for the LMT-20-II thruster is scaled from the design of the NASA SERT-II thruster. The magnetic endplate consists of two thin iron sheets rather than a single iron sheet of the minimum required thickness to link the magnetic flux. These sheets act as additional heat shields to further reduce the radiant coupling between the anode and cathode thermal circuits.

B. LM CATHODE K-54

Lightweight annular LM cathode K-54 was fabricated especially for use with the LMT-20-II system. This LM cathode is shown schematically in Fig. 11. It was designed specifically to take full advantage of operation with a single-capillary feed system and is attached to the removable portion of the aluminum backplate of the LMT-20-II system by studs which protrude from the back of the cathode. Only molybdenum surfaces are exposed to the discharge. Holes are provided through the cathode body to provide clearance for a discharge igniter electrode. The design of LM cathode K-54 differs from that of most previous high temperature LM cathodes in that the annular pool-keeping structure is formed from cylindrical rather than conical elements. While the performance of LM cathode K-54 was entirely satisfactory in operation of the LMT-20-II system, there are indications that the specific thermal loading $V_{K,th}$ of this cathode was significantly higher than has been measured earlier with cathodes having the conically shaped pool-keeping structure*. The conical configuration is best exemplified by the design of the LM cathode K-25-V which was described and tested extensively during the first phase of this contract.[1]

Because LM cathode K-54 was not available for testing outside of the LMT-20-II system, an alternate LM cathode K-51 (which employs an identical pool-keeping structure) was tested in its stead. Figure 12 is a photograph showing LM cathode K-51 mounted for testing in a diode discharge. A gas cooled metal heat sink is attached to the outer edge of the removable section of the thruster's aluminum backplate as a substitute for the heat sink normally provided by the thruster itself.

---

*$V_{K,th}$ is defined as the ratio: (thermal power $P_{K,th}$ received by the LM cathode from the discharge)/(electron current I_K delivered by the LM cathode to the discharge) or $V_{K,th} = P_{K,th}/I_K$.

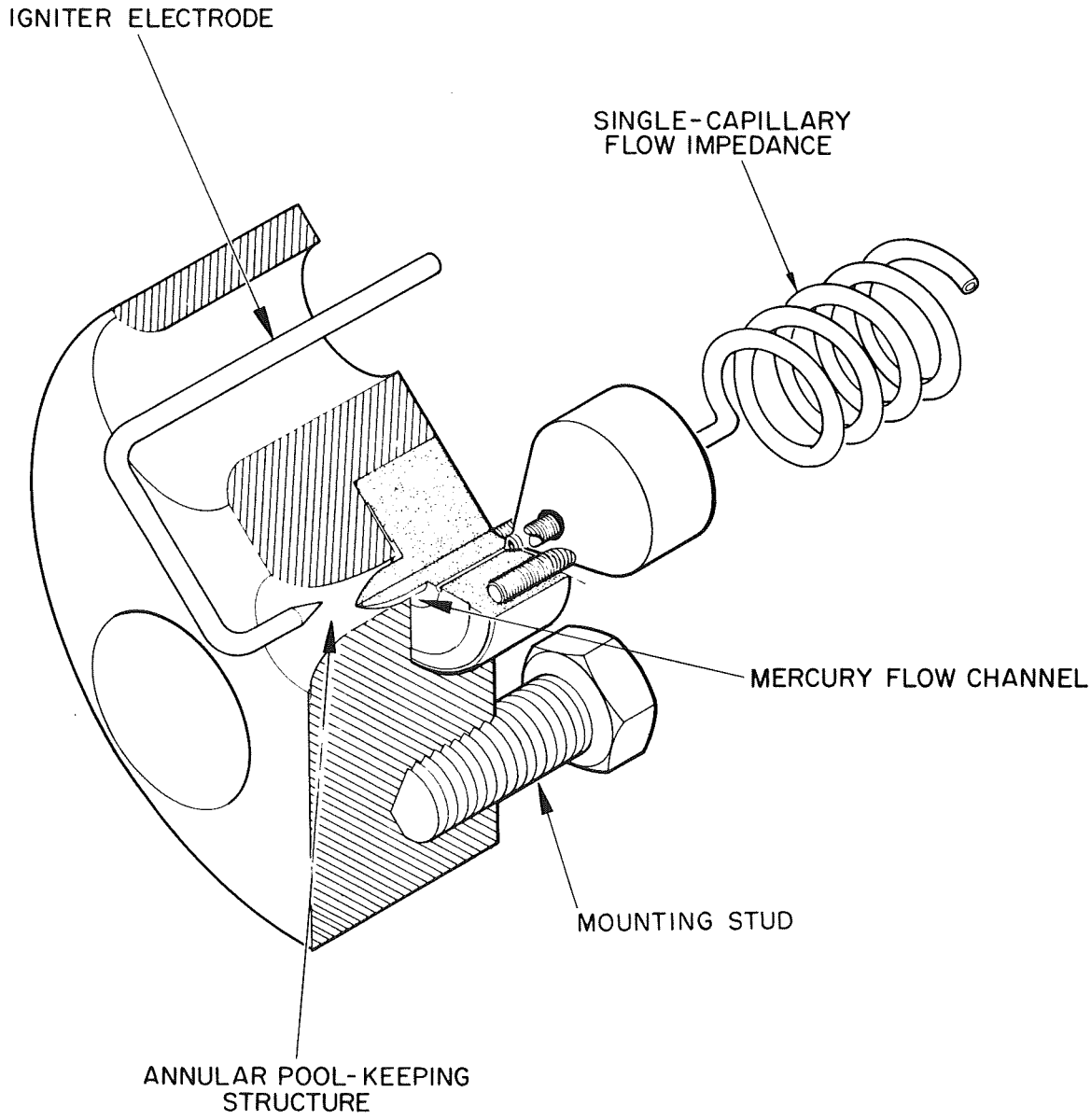

Fig. 11. LM cathode K-54.

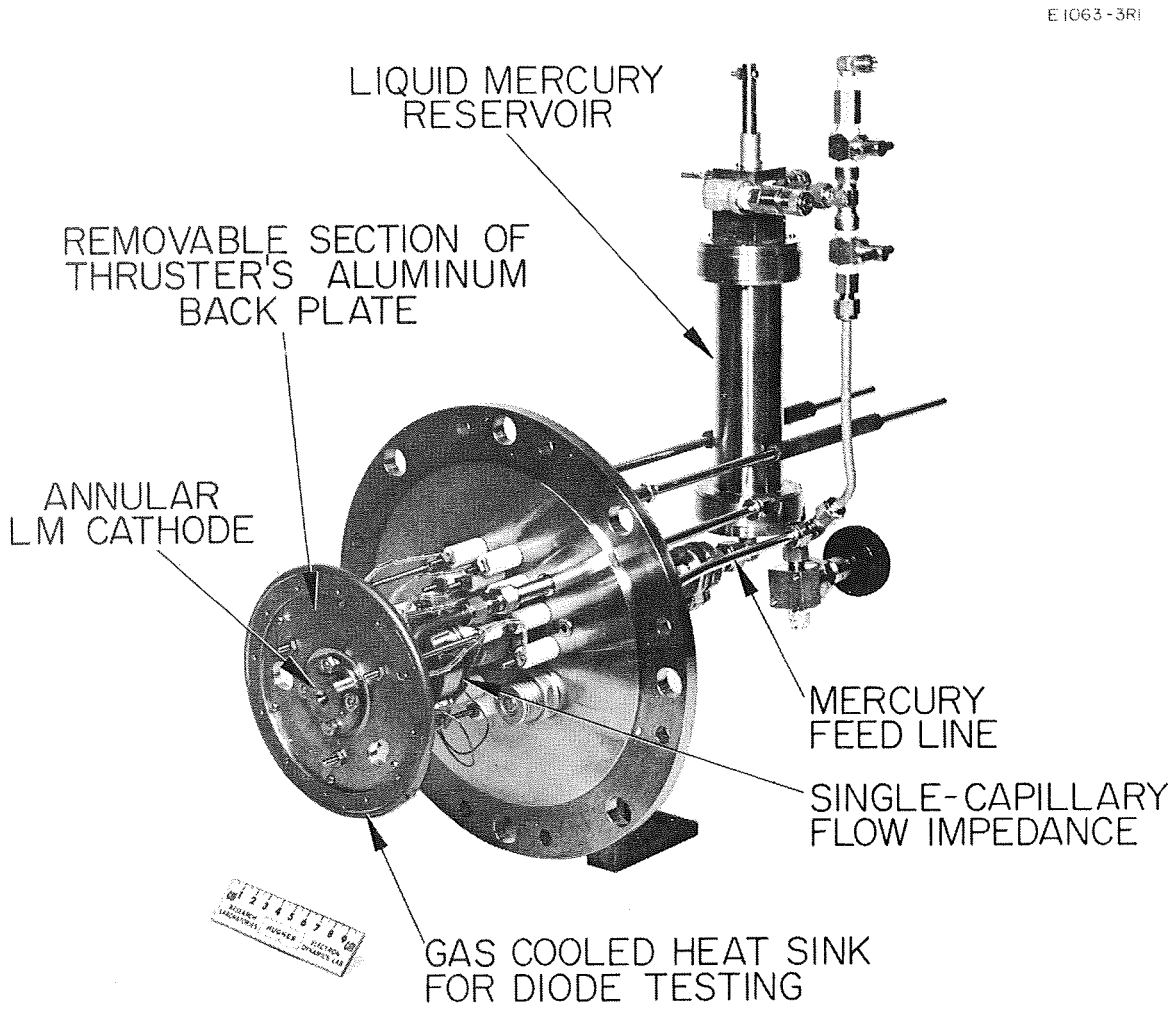

Fig. 12. LM cathode K-51 mounted for testing in a diode discharge.

The specific thermal loading of LM cathode K-51 was measured as a function of the cathode body temperature T_K. As shown in Fig. 13, the specific thermal loading at 155°C is equal to 4 W/A, but rises steeply for operation at temperatures above T_K = 200°C. It is clear that a wider latitude is available for efficient operation with LM cathode K-25-V. With a design incorporating the pool-keeping structure of LM cathode K-25-V into the outer body of K-54, a cathode embracing the best characteristics of both can be developed.

C. MERCURY FEED SUBASSEMBLY

To supply propellant to the LMT-20-II thruster, a prototype liquid-mercury feed system has been designed with emphasis on simple, reliable operation. As shown in Fig. 14, the system contains all elements necessary to provide mercury propellant for the thruster in a measured and controllable manner. In order of flow sequence, the liquid-mercury feed system includes a mercury shutoff valve, a hydrogen-bubble high voltage isolator, an EM pump, a mercury flowmeter, and a single-capillary impedance to regulate the mercury flow to LM cathode K-54.

The feed system is supplied with mercury by the gas pressurized mercury reservoir shown in Fig. 15. Pressurized nitrogen is applied above a piston pressing on the mercury surface to serve as the driving force. The piston position is indicated by a dial indicator (calibrated to 0.001 in. or 0.0001 in.) which contacts the top of the piston shaft. Its displacement as a function of time serves as an indication of mercury consumption and yields an accurate measure of the flowrate which supplements the instantaneous value obtained from the flowmeter. The shutoff valve permits handling of the thruster system outside the vacuum environment with no loss of mercury or atmospheric contamination of the stored mercury. The high voltage isolator permits

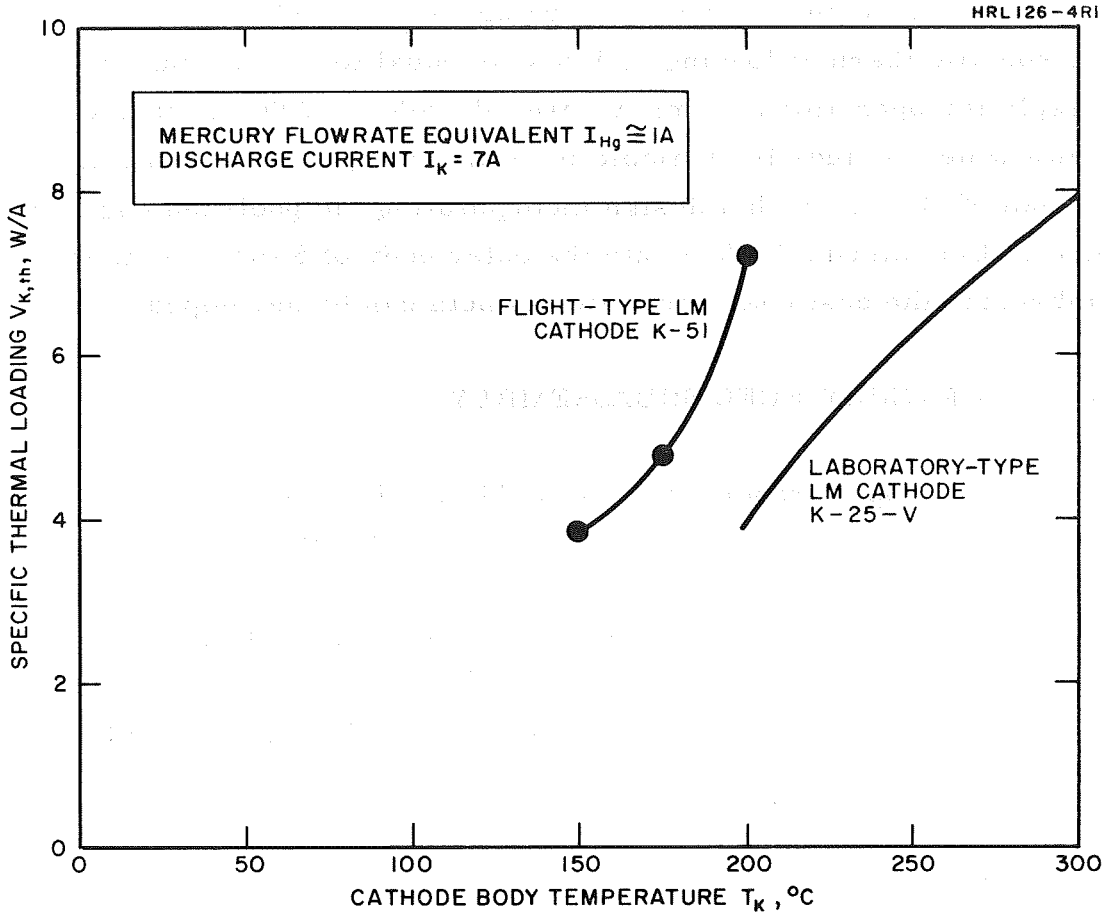

Fig. 13. Specific thermal loading as a function of the body temperature of LM cathode K-51 as compared with that of LM cathode K-25-V.

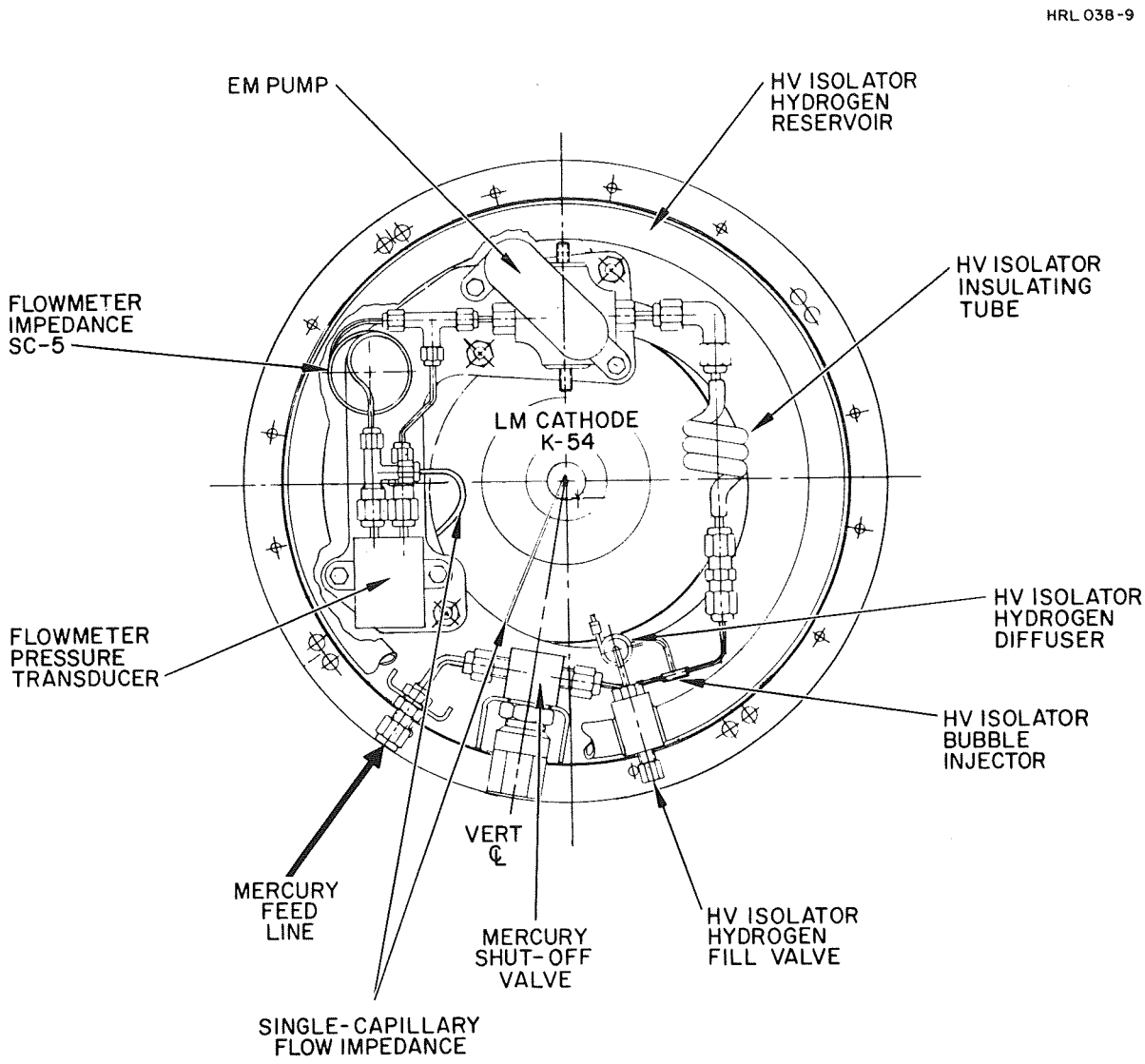

Fig. 14. Schematic drawing of the LMT-20-II mercury feed subassembly.

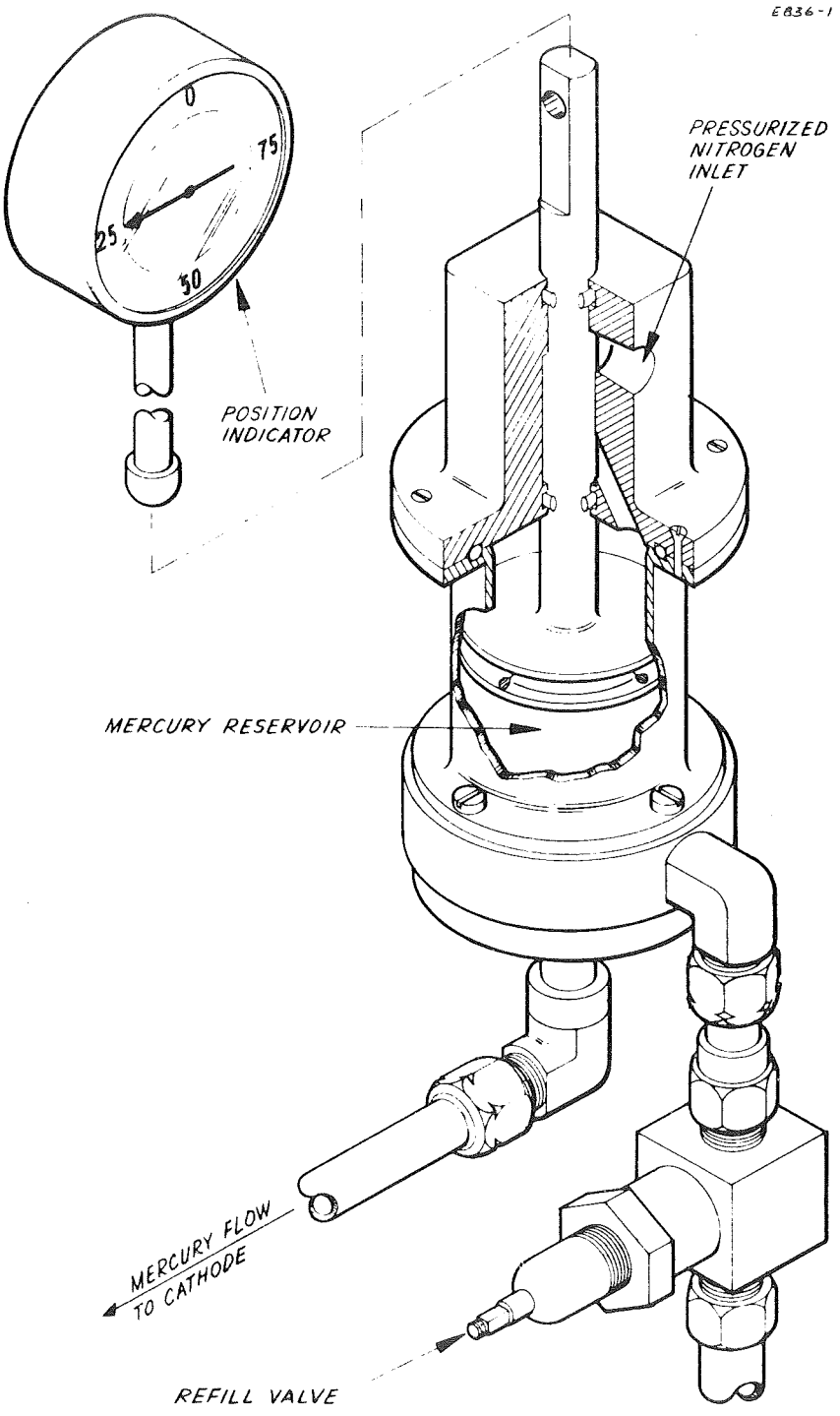

Fig. 15. Gas pressurized mercury reservoir.

operation of the thruster at a potential which is different from that of the propellant storage reservoir. Mercury pressure can be regulated, as needed to control the mercury flowrate, by means of an electromagnetic pump; the single-capillary flow impedance establishes a mercury flowrate which is linearly related to the applied pressure. The characteristics of the single-capillary flow impedance are sufficiently linear and repeatable to permit its use for both flow control and flow measurement.[1] A differential pressure sensor, which measures the pressure drop across a calibrated segment of the single-capillary flow impedance, provides an instantaneous electrical readout of the mercury flowrate. This electrical readout, combined with the capability for electrically actuated pressure regulation, permits ready implementation of automatic flow control.

1. Electromagnetic Pump

Mercury flowrate is regulated with an electromagnetic (EM) pump which is capable of producing a pressure difference of ±0.6 atm when driven at ±20 A. The electrical power consumption of the pump has been measured to be less than 2W. The over-all dimensions of the pump are 5 cm x 5 cm x 3.5 cm and its weight is 301 g. The pump has been operated satisfactorily for 800 hours with a total of 2.4×10^6 A-hours of mercury flow equivalent circulated through it.

The EM pump utilizes 0-ring seals between a nylon pump body and the current carrying electrodes, the magnetic pole pieces, and the mercury feed channels (see Fig. 16). Nylon with 20% glass reinforcing was employed because of its high strength, high service temperature, and low coefficient of thermal expansion, which makes it compatible with the thruster operating environment. Operation of the pump is similar to that of the design developed under Contract NAS 7-539 (Ref. 5), except that problems of leakage have now been eliminated.

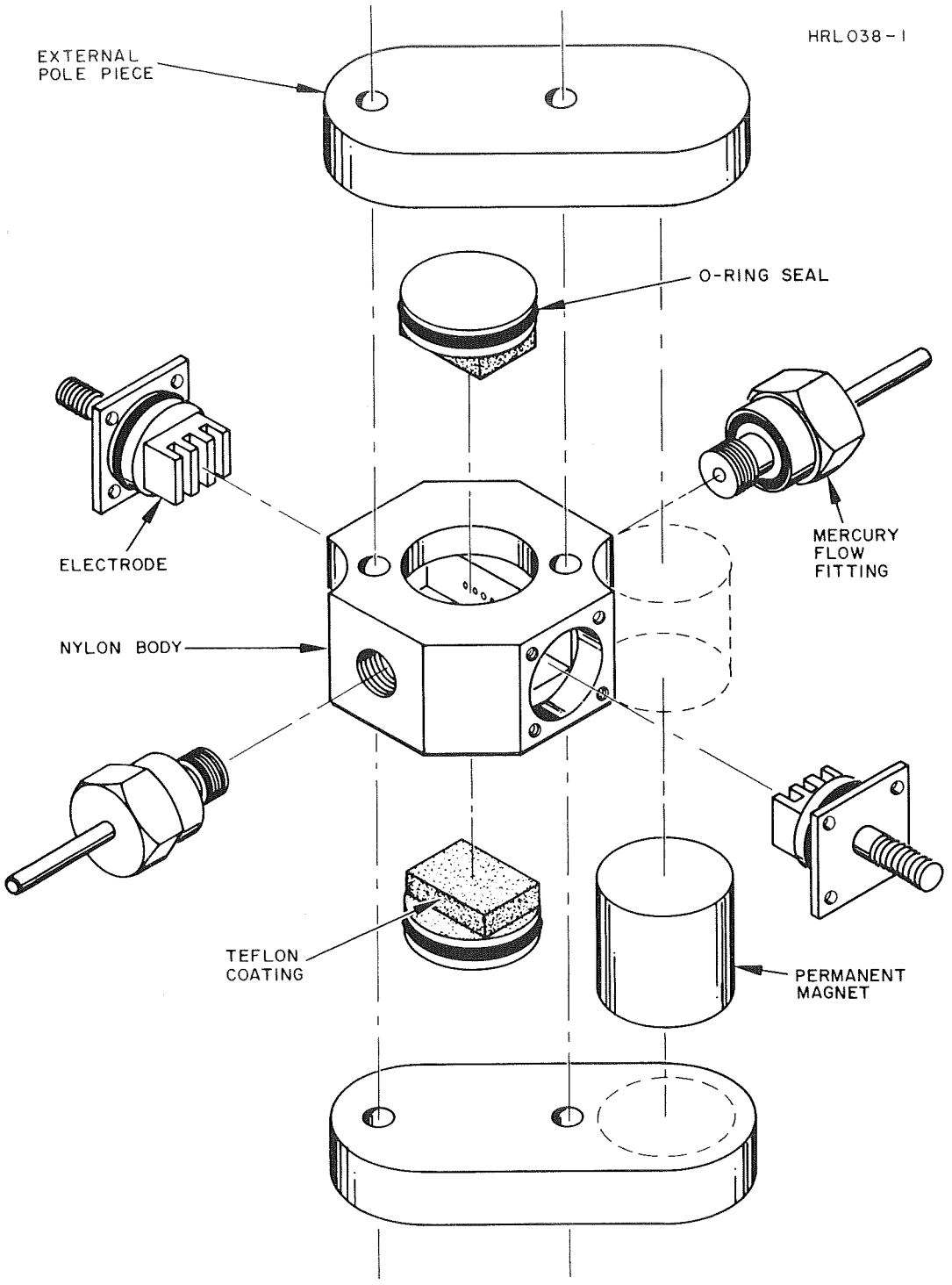

Fig. 16. Electromagnetic pump.

A magnetic field of 7 kG is concentrated into a narrow pumping region which is 0.025 cm wide and 1.27 cm on each side. Narrow channels are cut into the nylon pump body between the pumping region and the mercury feed line in order to discourage eddy currents in the mercury flow. The pole pieces have been coated with a thin layer of Teflon (0.003 cm thick) which is sprayed and baked onto the surface to provide electrical insulation from the mercury.

The electrodes which contact the liquid mercury are slotted to increase their surface area. The electrodes operated under Contract NAS 7-539 were plated with platinum so that they would be wetted by the mercury. Both features were incorporated in that effort to reduce the electrical resistance of the contact surface between the mercury and the electrode surface. The platinum plated electrodes performed satisfactorily throughout the testing of the prototype device under Contract NAS 7-539. After one year of storage and intermittent use, this pump was disassembled for inspection under the first phase of the current contract.[1] Although no degradation in performance was observed either before or after that time, some pitting of the platinum plated surface was noted. Thus there was some apprehension concerning the long term integrity of a platinum surface under possible attack by mercury. The electrodes used in the current pump design are fabricated of molybdenum, a material which simultaneously provides low contact resistance and offers total assurance of long life operation. The low contact resistance of molybdenum electrodes is related to the superior mercury-wetting characteristics of the molybdenum surface. The voltage drop across the pump is reduced to the value imposed by the resistance of the mercury alone when molybdenum electrodes are used.

In a preliminary life-test, the EM pump with molybdenum electrodes was subjected to 800 hours of operation at 20 A electrical current while circulating mercury through it in a vacuum environment.

With the mercury flow set at an equivalent rate of approximately 3000 A, a total of 2×10^6 A-hour of mercury flow equivalent was circulated through the pump during the test. During the first 450,000 A-hours, the voltage across the pump remained at a minimum value. During the next 1,000,000 A-hours, however, the voltage rose slowly, leveling off finally at a value of slightly less than 0.5 V. After reaching this maximum value, the voltage drop across the pump began to decrease slowly throughout the duration of the test. When the test was terminated, the voltage drop had decreased to 0.35 V.

Accompanying the voltage fluctuations, small bubbles of gas appeared on the surface of the glass tube which formed the mercury flow circuit. Since the entire flow system was enclosed within a vacuum environment, it was presumed that the source of the gas was from atmospheric elements dissolved within the liquid mercury itself. Even though the mercury had been triply distilled under vacuum prior to purchase, sufficient time had elapsed for atmospheric gases to be absorbed by the mercury during storage.

A second life-test indicated that gas bubbles dissolved within the mercury were in fact the primary cause for the increase in internal resistance of the EM pump which was observed during the first life-test. The same pump used during the first 800 hour life-test was disassembled and the electrodes were cleaned and replaced. The glass tubulation forming the mercury flow circuit was modified so that liquid mercury could be distilled and condensed into the flow system in a vacuum environment of 10^{-5} Torr. The pump was subsequently operated for 800 hours, with a total of 2.4×10^6 A-hours of mercury flow equivalent circulated through the pump, as in the previous test. During the entire test, the voltage drop across the pump increased only slightly from 0.076 V to 0.097 V at an electrical current flow of 20 A.

2. Mercury Flowmeter

During the first phase of this contract, mercury flowrate through a single-capillary flow impedance was shown to be a linear function of the pressure drop across its length.[1] This characteristic was exploited under the present effort by the development of a mercury flowmeter which utilizes a differential pressure transducer to measure the pressure drop across a calibrated section of the capillary flow impedance. For initial testing, a Winsco Model PB415 differential pressure transducer* was used which yields a 25 mV signal output for an applied pressure difference of 10 psi. The transducer output is linear and repeatable to within 1% of full scale. This transducer was used to measure the pressure drop across a single-capillary flow impedance, designated SC-5, consisting of a 915 cm length of 0.0178 cm i.d., Type 304 stainless steel tubing. Impedance SC-5 was attached to the upstream end of single-capillary flow impedance SC-3 (1,060 cm length of 0.014 cm i.d., Type 304 stainless steel tubing) to simulate the flow impedance leading to an LM cathode.

The flowmeter was calibrated by correlating the electrical output signal of the pressure transducer with the mercury flowrate, which was determined by the rate of displacement of the piston of the gas pressurized mercury reservoir. Data points were acquired at a rate of only one or two per day to insure that each value of the mercury flowrate would be determined to the same high accuracy anticipated from this instrument. The initial first ten data points confirmed the high expectations held for the flowmeter, exhibiting a linear output characteristic with a signal amplitude of 24 mV per ampere equivalent

*This was replaced by a lightweight Whittaker Model P109D pressure transducer in the final LMT-20-II package to reduce system mass.

of mercury flow within a standard deviation of ±1% over the range from 0.2 A to 1.2 A. The first ten data points are indicated as solid circles in Fig. 17. The next seven data points, indicated as open circles, showed a marked increase in scatter as the calibration characteristic underwent a change to a new value which is described by the next 16 data points, indicated by solid triangles. The new calibration characteristic was also linear with an output signal of 24 mV/A equivalent with a standard deviation of slightly greater than ±1%, but it now exhibited a different intercept of transducer output for zero flowrate; whereas initially the pressure drop across capillary SC-5 approached a value 1.7 psi for zero flowrate, the value of the intercept shifted in time to a value of 2.5 psi. The reason for this shift in intercept and, in fact, for the existence of a nonzero intercept in the first place is discussed in the appendix of Ref. 8. The existence of a nonzero intercept is believed to indicate the presence of minute gas bubbles which are lodged within the liquid-mercury feed system. If these gas bubbles were not present, the pressure drop across capillary SC-5 would approach zero for zero flowrate, and no fluctuations could occur.

In order to eliminate time variations in the flowmeter calibration for future testing, an apparatus to distill mercury under vacuum was constructed. With this unit (which was employed in preparation for demonstration of the LMT-20-II system), the mercury distillate is collected directly within the feed-system reservoir where it is kept from contact with atmosphere up to the time that it is consumed in the thruster discharge.

3. Hydrogen-Bubble High Voltage Isolator

The LMT-20-II thruster is isolated from the mercury storage reservoir by the use of a hydrogen-bubble high voltage (HV) isolator. In this device, a small hydrogen bubble is introduced into the mercury flow stream within an insulated tube. Previous efforts with a

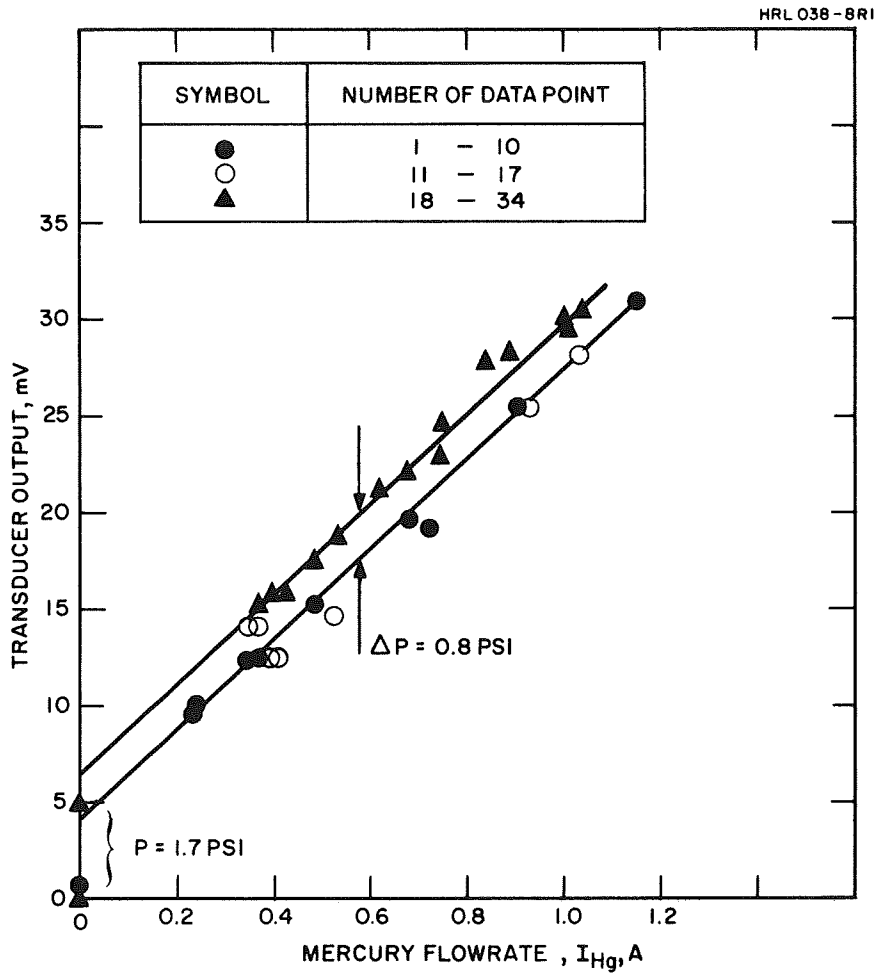

Fig. 17. Mercury flowmeter calibration characteristics.

hydrogen-bubble isolator utilized a Teflon insulating tube.[1,5] With this design, the bubble was observed to decrease in length as it passed through the insulated section of the tube. An initial requirement for a new isolator design was to determine the cause of hydrogen loss.

Experiments were conducted which demonstrated that loss of hydrogen gas was due to diffusion through the walls of the teflon tubing rather than by absorption into the mercury.[8] In the same experiments, the rate of diffusion through walls of either glass or alumina tubing was found to be entirely acceptable. On this basis, an experimental model of the HV isolator was constructed with an insulating tube made of glass. The experimental assembly, shown in Fig. 18, incorporates fittings which permit interchange of alternative insulating tube sections and utilized a commercially available high pressure reservoir for hydrogen storage.

Satisfactory performance was demonstrated by operation of the experimental model of the HV isolator. This isolator employed an iron diffuser element to regulate the flow of hydrogen gas which enters the mercury flow stream as it passes through a section of flow line. To initiate operation of the isolator assembly for the first time, the temperature of the diffuser element was adjusted to a value at which the hydrogen bubbles were injected into the mercury stream with a length of 1 cm. After 20 hours of operation (overnight), the bubble length had increased to approximately 10 cm as a result of increased hydrogen flowrate caused by conditioning or flushing of the diffuser element. Following this initial startup transient, the temperature of the diffuser element was lowered to a level at which bubbles of 1 cm length were again produced. After 80 hours of subsequent operation, with no further adjustments in the diffuser temperature, operating characteristics of the HV isolator were investigated as a function of the temperature of the diffuser element and the mercury flowrate.

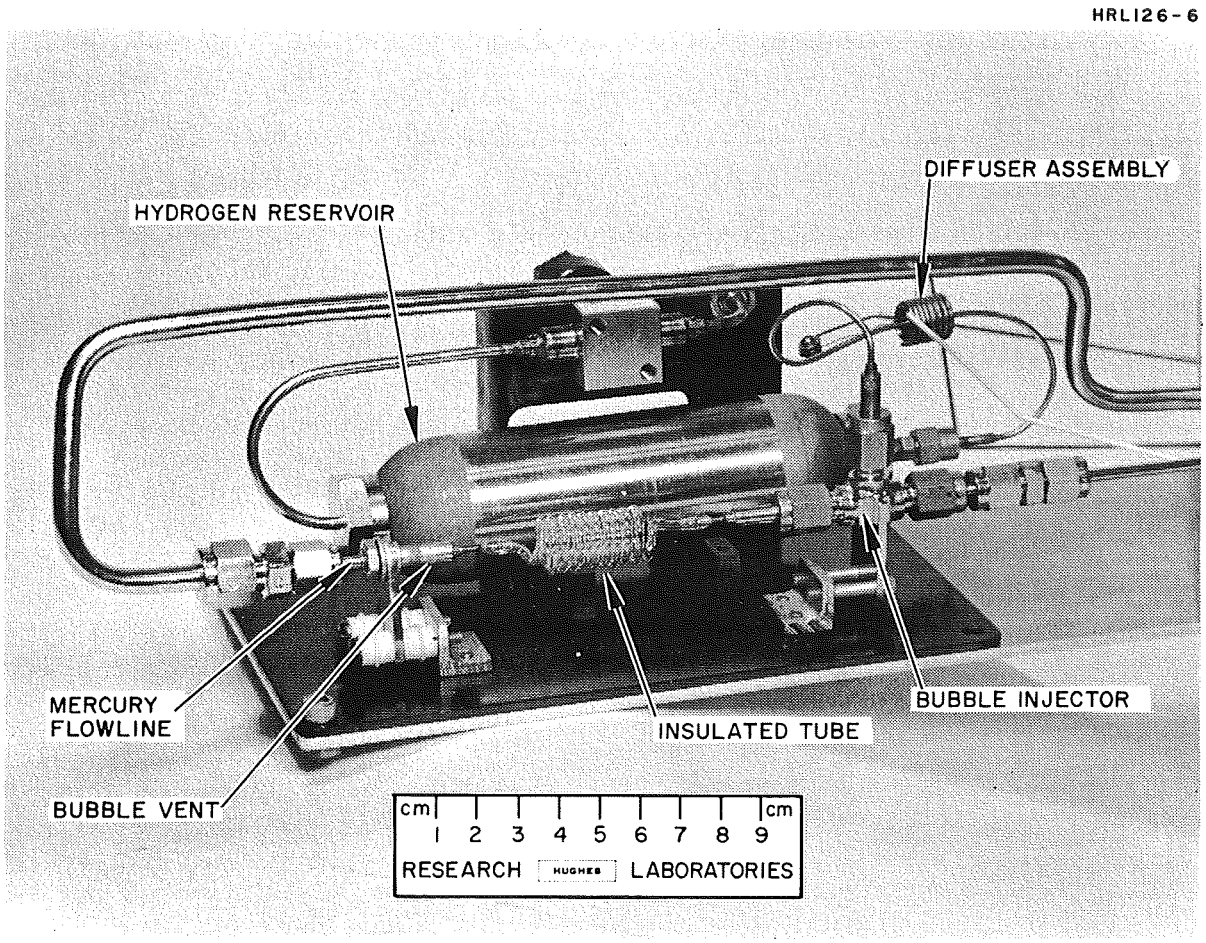

Fig. 18. Experimental model of the high voltage isolator assembly.

The HV isolator was operated first at a bubble production rate of 4 bubbles/hour. At a mercury flowrate equivalent I_{Hg} = 0.6 A, a standby power level of 1.5 W combined with 2 min power pulses each quarter hour of 4.8 W was sufficient to inject hydrogen bubbles which are 1 cm long (see Fig. 19). The temperature of the diffuser element varied between 315° and 390°C under the conditions of the test, which was conducted with an ambient background temperature of 30°C. At a mercury flowrate equivalent I_{Hg} = 1.25 A, equivalent performance was achieved by raising the standby power level to a value of 2.2 W, while leaving the 2 min power pulses at a level of 4.8 W.* At this increased power level, the temperature of the diffuser element varied between 350° and 395°C.

In a second mode of operation, the production rate was reduced to 2 bubbles/hour and no standby power was employed. These simplifications were made possible by taking advantage of the long thermal response time of the diffuser assembly. To produce hydrogen bubbles which are 1 cm long, 2 min pulses of 5.5 W and 7.0 W were required for mercury flowrate equivalents I_{Hg} = 0.6 A and 1.25 A, respectively. The required power levels resulted in a temperature variation of the diffuser element of from 150° to 295°C at I_{Hg} = 0.6 A, and from 160° to 320°C at I_{Hg} = 1.25 A under the test conditions.

*The required increase in standby power with increased flowrate was necessary with the experimental setup only, and is not required in operation of the complete LMT-20-II mercury flow system. This increase compensates for the greater driving pressure at the isolator location which is associated with increased flowrate which otherwise tends to reduce the bubble length. In the LMT-20-II system, pressure variations are induced by means of the electromagnetic pump located downstream of the HV isolator.

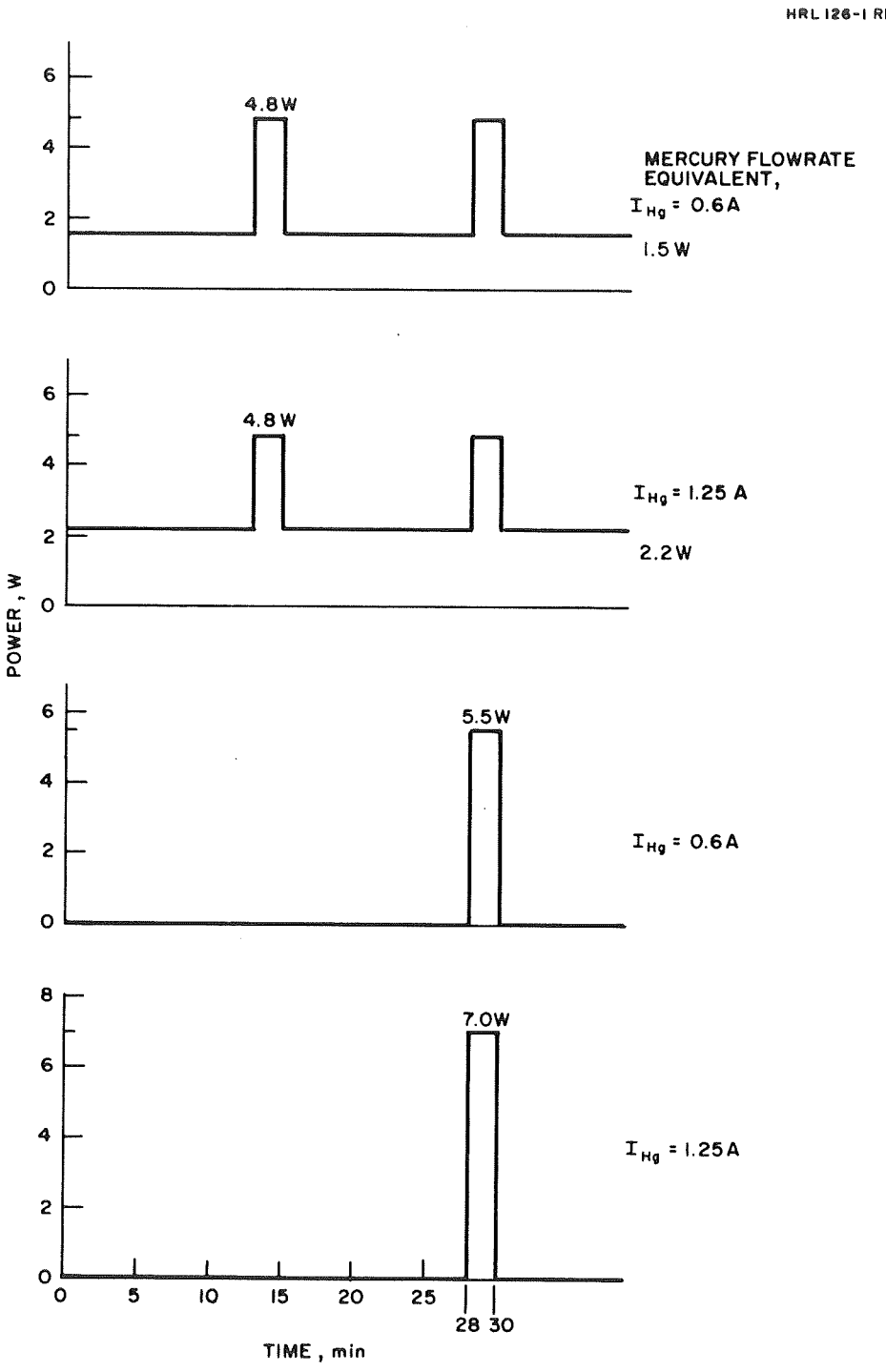

Fig. 19. Power levels required for production of 1 cm long hydrogen bubble.

The HV isolator was operated continuously for 350 hours while its operating characteristics were determined. An additional 200 hours of running time has been accumulated in the second mode of operation (which requires no standby power) with high voltage (2 kV) applied. The effectiveness of the isolation was monitored with a strip-chart recorder, and no short circuits were observed during this time.

The experimental isolator was turned off several times in order to observe the transient operating characteristics during startup. When the isolator is started (in the mode requiring no standby power), the diffuser element approaches its maximum operating temperature after the first power pulse, and a bubble is produced. The first bubble passes out of the injector region and into the insulated tube after a time of from 10 to 20 min, depending on the mercury flowrate. Operation proceeds normally thereafter.

In operation of the LMT-20-II system, the flight-type HV isolator operated automatically and flawlessly in the mode where no standby power is required. This unit employed an alternate reservoir design (shown in Fig. 8) which was 70% lighter than the commercial reservoir. It is fabricated of titanium and features welded joints, lightweight input and output terminations, and a toroidal construction for a better fit into the feed subassembly package. The titanium reservoir was filled with hydrogen gas to a pressure of 400 psi.

D. POWER CONDITIONING

An all solid-state power conditioning subsystem was constructed which contains the electronic circuitry necessary to provide appropriate power inputs (from a solar array power source) for the EM pump and the high voltage isolator of the LMT-20-II feed subassembly. The subsystem consists of a solar panel simulator, a voltage regulator, a 10 kHz converter, a power control circuit for the EM pump, and a power

controller for the high voltage isolator. Each part of the subsystem was built as a separate module. A circuit diagram is given in Fig. 20, which shows each of the circuits and the cable connections joining them. The solar panel simulator provides an output voltage of 60 to 90 V dc (dependent on load) to simulate a solar panel operating in space. The voltage regulator provides a 60 V dc output which is regulated to within ±2%. From this signal, the converter produces plus and minus 15 V dc voltages for use by the EM pump power system and 60 V square wave power at 10 kHz for use by both the EM pump and high voltage isolator systems.

The ultimate output of the EM pump power system is a variable dc voltage in the range -0.1 V to +0.1 V; its magnitude and polarity are determined by the magnitude and polarity of a control signal which can be either a reference signal or the feedback command input provided by the liquid-mercury flowmeter developed under this contract. The isolator system provides 15 V pulses of 10 kHz power to drive the heater, which is located in the iron diffuser element of the hydrogen-bubble high voltage isolator. The time between pulses is 30 min, and the pulse width is variable from 10 sec to 2.8 min.

The apparent complexity of the circuit shown in Fig. 20 reflects the wide versatility designed into the laboratory supply and does not represent an actual complexity for flight-type equipment. To illustrate the difference, two configurations are shown in Fig. 21, for the EM pump power conditioning circuit. In the laboratory configuration, provision has been made for continuous transition from an output of +0.1 V to -0.1 V into the EM pump. The output is virtually ripple free being generated by full wave rectification of the 60 kHz square wave power by transistor switches which are operated with two in parallel to accommodate large currents with a conservative design. In the flight-type design, on the other hand, only two transistors and one operational amplifier are used. The operational amplifier compares

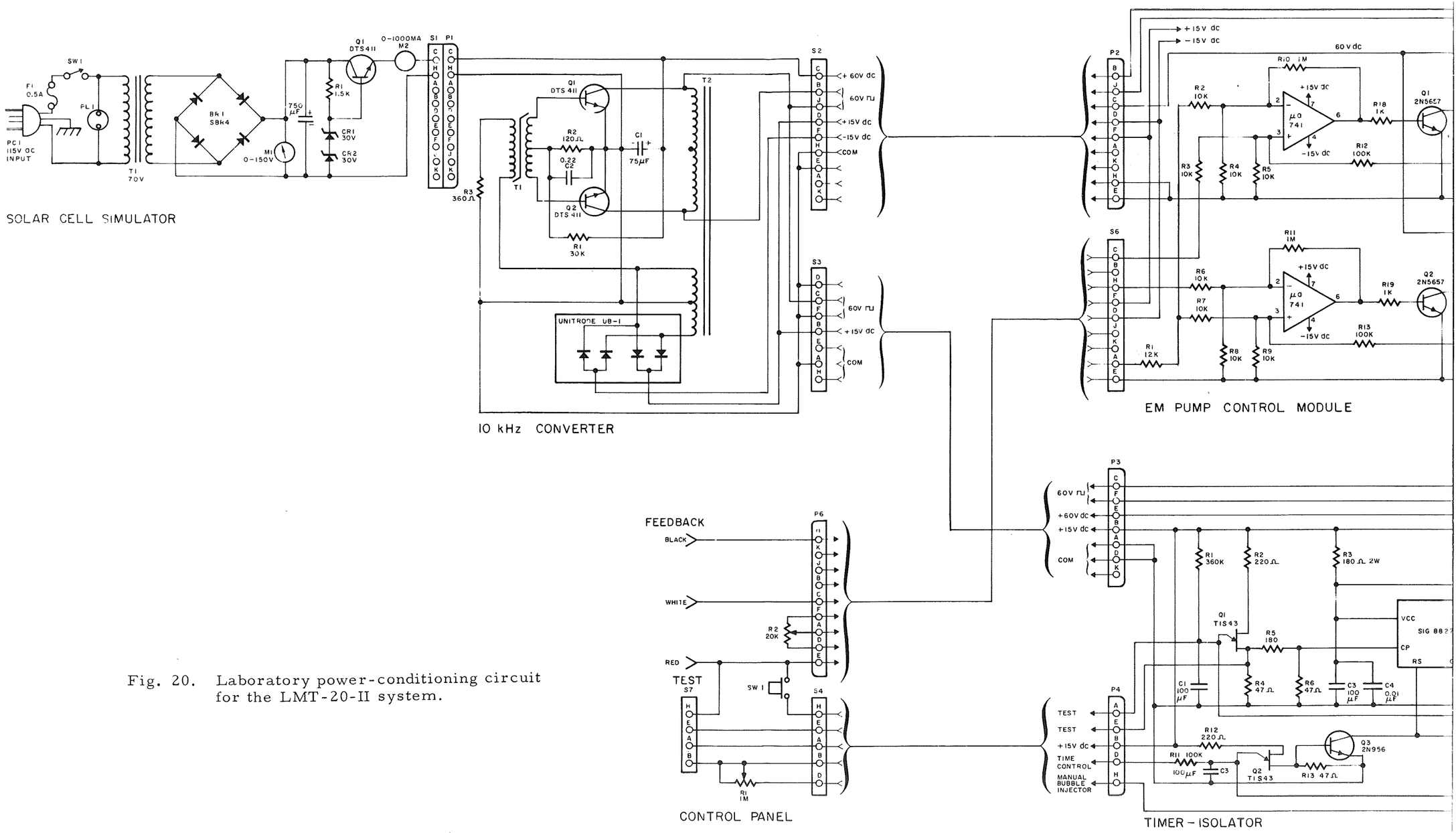

Fig. 20. Laboratory power-conditioning circuit for the LMT-20-II system.

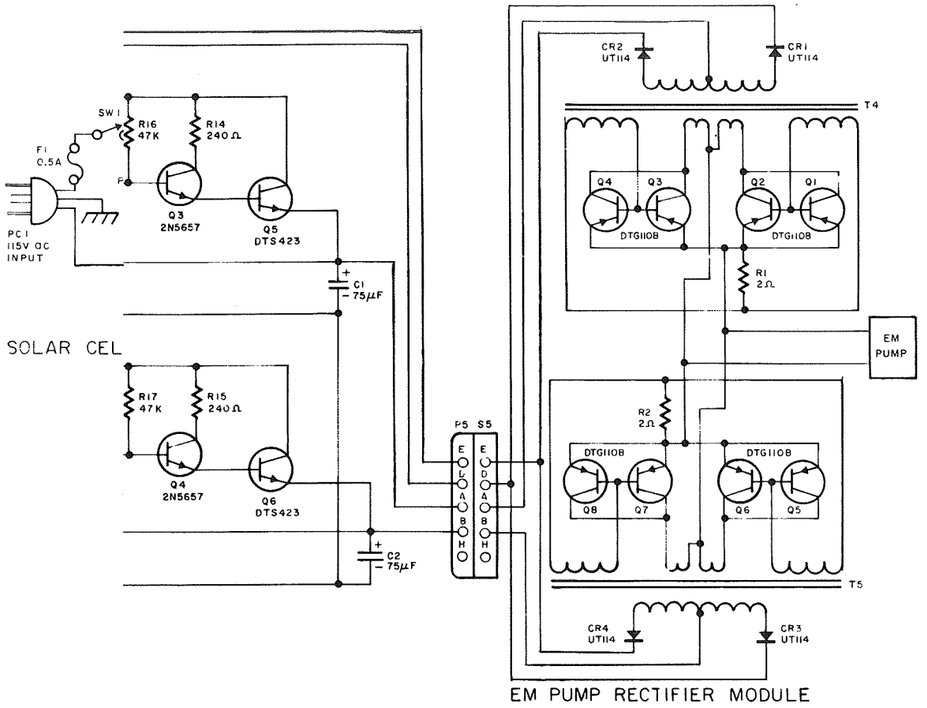
CR2 UTI14
CR1 UTI14
T4
SW1
R16 47K
R14 240Ω
F1 0.5A
Q4
Q3
Q2
Q1
DTGII0B
DTGII0B
Q3 2N5657
Q5 DTS423
PC1 115V QC INPUT
C1 75μF
RI 2Ω
EM PUMP
SOLAR CEL
R17 47K
R15 240Ω
P5 S5
R2 2Ω
DTGII0B
DTGII0B
Q4 2N5657
Q6 DTS423
Q8
Q7
Q6
Q5
C2 75μF
T5
CR4 UTI14
CR3 UTI14
EM PUMP RECTIFIER MODULE

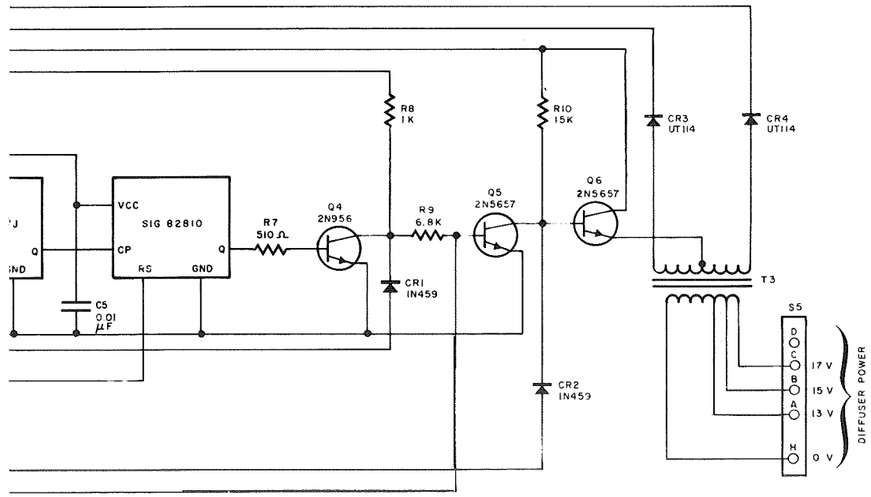
R8 1K
R10 15K
CR3 UTI14
CR4 UTI14
VCC
SIG 82810
CP
RS
GND
Q
R7 510Ω
Q4 2N956
R9 6.8K
Q5 2N5657
Q6 2N5657
CR1 IN459
C5 0.01 μF
T3
S5
17 V
15 V
13 V
0 V
DIFFUSER POWER
CR2 IN459

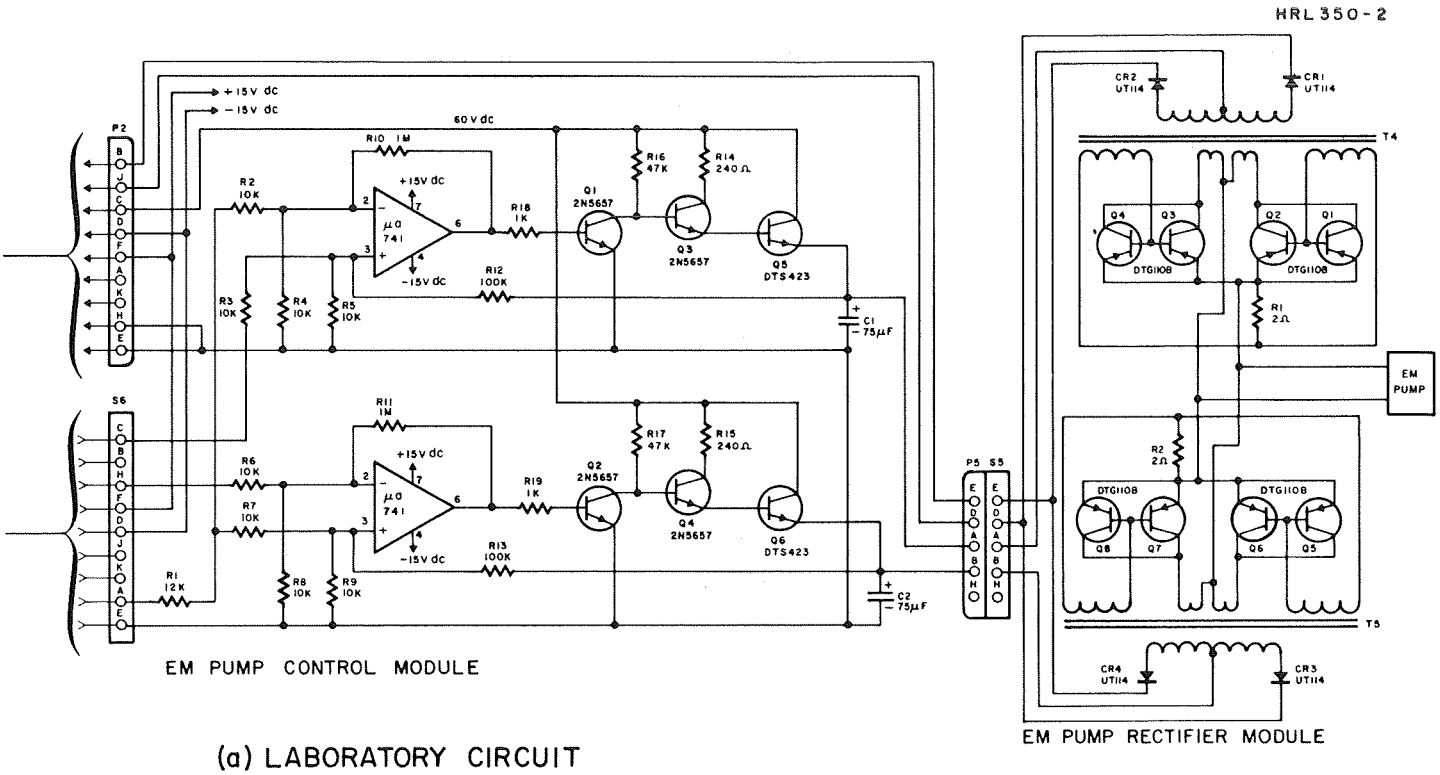

(a) LABORATORY CIRCUIT

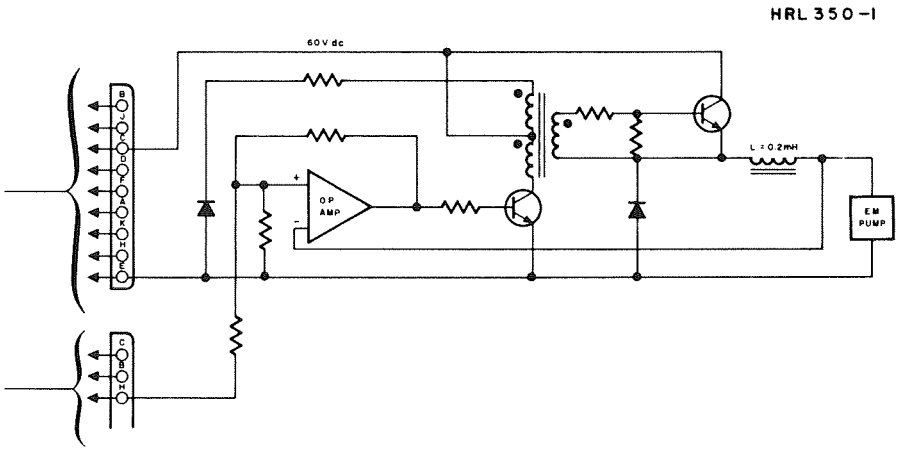

(b) FLIGHT-TYPE CIRCUIT

Fig. 21. EM pump power conditioning circuits.

the output voltage (proportional to the current across the EM pump) to a command set point. When the current falls below the value required, the operational amplifier operates as a Schmidt trigger circuit to connect a 60 V dc supply voltage through a 0.2 mH choke to the EM pump. The current through the pump rises, in response to the supply voltage, to the value which is required to switch off the Schmidt trigger. This circuit is not designed for operation with plus and minus current flow, but this capability could easily be implemented if desirable. A ripple of about 10% of the full scale output has been permitted in the flight-type supply, because high frequency fluctuations in pump power (resulting from the power supply ripple) do not result in any significant fluctuation in the mercury flowrate. This is so because of the integrating effect which occurs at the LM cathode by accumulation of mercury in the pool-keeping structure.

SECTION V

THERMAL ANALYSIS

Detailed thermal analysis is required to establish accurate quantitative criteria for the design of a lightweight thermally integrated LM cathode thruster. The first detailed analysis of an electron bombardment thruster was undertaken at HRL under Contract JPL 952129, in which a thermal simulation of the ion-extraction system was carried out. Because of the limitations of that program, the simulation did not include the discharge chamber.

A complete thermal simulation of the thermally integrated LM cathode thruster has been undertaken as part of the present effort. This work involved the following tasks: (1) carry out a detailed thermal simulation of the discharge chamber of a thermally integrated LM cathode thruster, (2) combine the simulations of the discharge chamber and ion-extraction system, (3) compare the predictions of the thermal simulation with temperatures measured experimentally with the LMT-30-I thruster to improve the accuracy of thermal simulation, (4) use the proven simulation to analyze the thermal characteristics and improve the design of the LMT-20-II thruster, and (5) correlate the calculated thermal data with temperatures measured experimentally with the LMT-20-II thruster in order to evaluate the thermal design.

Computer program TAS-1B, which was employed to thermally simulate the discharge chamber, is a digital computer program which solves for the steady-state temperature distribution in a lumped parameter network of temperature points (nodes) and heat flow paths (resistors). The inputs to TAS-1B which are required to model a device are the heat losses, nodal areas, radiant emissivities, radiation view factors, and thermal conductances. The heat inputs are determined for the most part from physical considerations which are based on an extension of a theory of discharge mechanisms which was

developed at HRL.[9] General relationships have been determined to facilitate calculation of the remaining quantities for a discharge chamber model comprising 28 nodes.

The geometrical configuration of nodes which is utilized to describe the thermal characteristics of the LM cathode thruster must be sufficiently similar to the actual thruster design to provide an accurate simulation, yet simple enough to provide a tractable theoretical problem. Figure 22 illustrates the system of nodes which is used to model the thermal properties of the thruster geometry illustrated in Fig. 10. Nodes 1 to 28 represent the discharge chamber and its ground-screen shroud, nodes 29 to 49 represent the ion-extraction system studied previously under Contract JPL 952129, and nodes 50 to 52 simulate the thruster environment. The problem is made more readily tractable by employing a number of assumptions. In modeling the discharge chamber it is assumed that the cathode-cup pole piece and propellant distributor baffle can be neglected in the configuration of nodes. Their influence can be taken into account by the appropriate calculated heat inputs to be discussed later. The anode connector is assumed to have the same outer diameter as the body of the thruster and to conduct a small quantity of heat to the body. The associated thermal conductance is assumed to be equal to that calculated for the thin stainless steel wall through which the anode connector studs pass. This assumption is based on the supposition that the stainless steel wall is in good thermal contact, through radiation transfer, with the front section of the anode and anode connector. It is also assumed that the ground screen has a fractional open area of f_s, and that it lies very close to the thruster body. The influence of multiple heat shields (e.g., between the thruster walls and the anode) is taken into account through calculated effective emissivity ϵ_e given by

$$\epsilon_e = \frac{2\epsilon}{(2 - \epsilon)(n + 1) + \epsilon} \quad ,$$

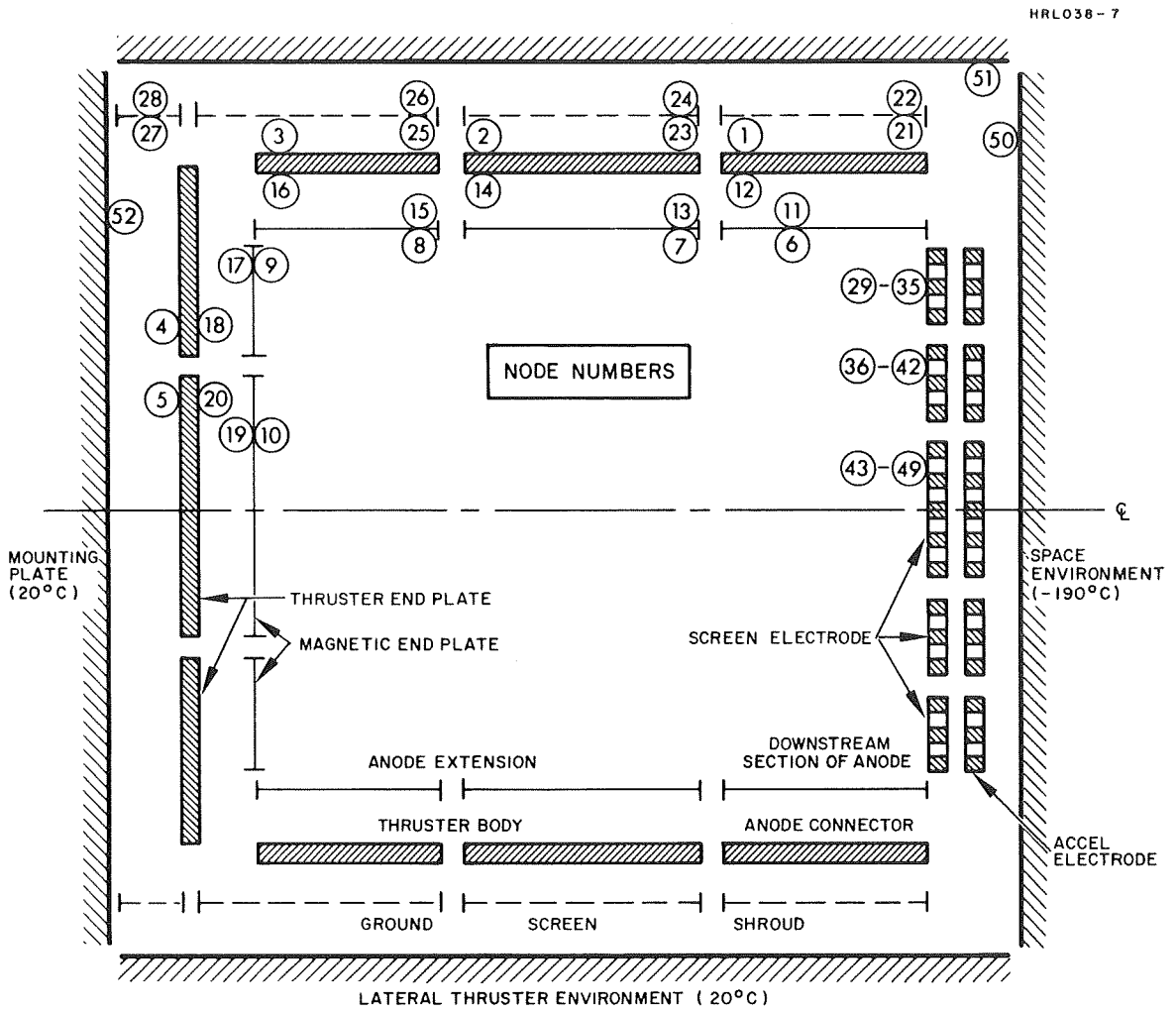

Fig. 22. Configuration of nodes used to simulate the thermal characteristics of an LM cathode thruster. The numbering of nodes is indicated in the upper half of the schematic.

where ϵ is the actual emissivity of one of the heat shield surfaces (all involved surfaces are assumed to have the same emissivity) and n is the number of heat shields.

The method of modeling the ion-extraction system was described in Ref. 10. Under Contract JPL 952129 the extraction system was divided into three concentric rings, as shown in Fig. 23. There is no thermal conduction between screen and accel electrodes, and only directly opposed rings are assumed to be coupled by radiation. The adjacent rings of any one electrode are coupled by conduction. Associated with each of the three rings are seven nodes, as illustrated in Fig. 23.

The thruster environment has been simulated in a manner which will allow the investigation of a number of possible situations. Node 50 represents the space environment, which has a fixed temperature and an emissivity of one. Node 51 also represents the space environment when the lateral surfaces of the thruster are exposed to space, but it can simulate the environment of a densely packed thruster array when its emissivity is set at zero. Node 52 can be made to represent an adiabatic wall when its emissivity is set at zero, or it can absorb radiation when a nonzero emissivity is used.

Calculation of the nodal areas, thermal conductances, and view factors for radiation transfer between each node and all other nodes is tedious but straightforward. The procedure is illustrated in Ref. 10. General relationships for the various quantities have been derived and a small computer program has been written which is employed to calculate values for any given dimensions and thermal conductivities. These quantities, along with the emissivities, heat inputs, and temperatures of fixed temperature nodes, constitute the inputs for computer program TAS-1B.

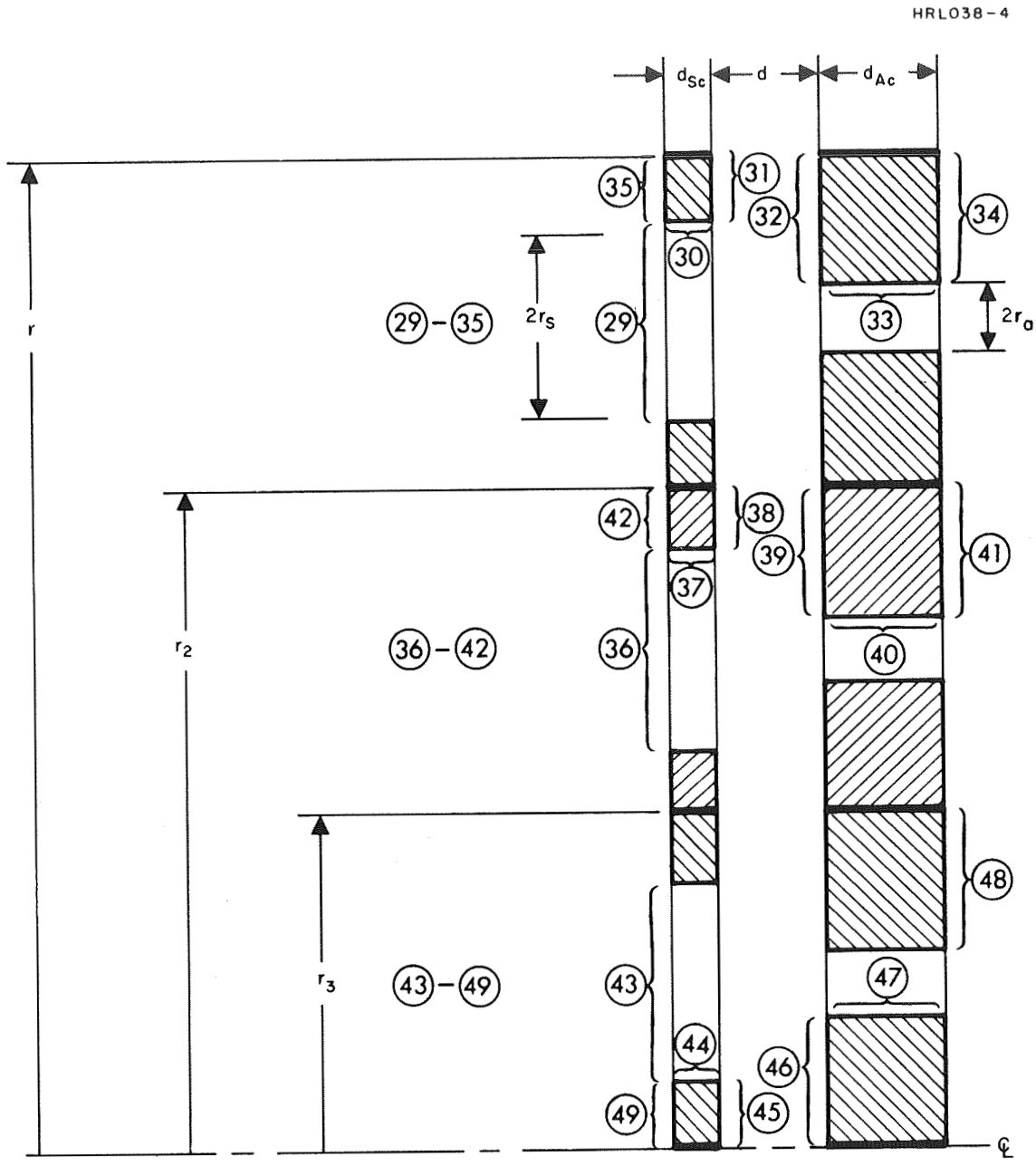

Fig. 23. Configuration of nodes used to simulate the thermal characteristics of the ion-extraction system.

A. DISCHARGE CHAMBER HEAT DISTRIBUTION

A physical theory which postulates a discharge mechanism for the electron-bombardment thruster has been developed at HRL[9] for determining the limits of power efficiency of these thrusters. In the following discussion, an analysis is presented in which these physical considerations are employed and extended to determine the distribution of heat inputs to an LM cathode thruster arising from discharge chamber losses.

The following conditions are assumed to apply to the LM cathode thruster.

- The plasma is uniformly distributed within the discharge chamber.
- The plasma electrons in the discharge chamber possess a Maxwellian energy distribution with a temperature T_p constant throughout the chamber.
- The plasma potential in the discharge chamber is uniform at a value ΔV_A above the anode potential V_A, except for positive potential barriers and sheaths near walls.
- The ion-extraction screen is at cathode potential and permits passage of a fraction α of the arriving ions. The remaining fraction $(1 - \alpha)$ is neutralized upon impact, and reenters the discharge traveling in the upstream direction.
- The endplate of the discharge chamber is held at cathode potential and all impacting ions recombine and come off as neutrals.
- Ions are prevented from reaching the anode. This assumption is based on the plasma probe measurements (by Eckhardt, et al.,[3] with an LM cathode thruster and by Knauer, et al.,[11] with both hollow- and oxide-cathode thrusters) which indicate the existence of a small positive potential ridge near the anode. This ridge prevents the impingement of ions originating at the center of the discharge chamber.

For the LM cathode, the following specific assumptions are made.

- A uniform plasma exists within the cathode-cup pole piece which has a potential V_C relative to the cathode and a Maxwellian electron energy distribution of temperature T_C.
- Energy is delivered to the cathode-cup plasma by electrons which accelerate from the cathode into this plasma. This energy goes into (1) releasing electrons from the liquid mercury surface, (2) heating of the cathode, (3) thermal energy of primary electrons which leave the cathode cup, and (4) heating of the cathode cup.

Employing these assumptions, the minimum total source energy per beam ion $V_S|_{min}$ for an electron-bombardment thruster has been shown[9] to be equal to

$$V_S\Big|_{min} = \frac{\beta\delta}{\eta_m} V_A + \left(\frac{\delta}{\eta_m} - 1\right) V_A \quad . \tag{1}$$

The terms introduced in this equation are defined below:

The quantity

$$\beta = \frac{\text{minimum number of primary electrons}}{\text{ionization}} = \frac{\text{energy consumption per ionization}}{\text{maximum energy available from primary electron}}$$

or

$$\beta = \frac{eV_i + e\Delta V_A + \frac{3}{2}kT_p + \frac{1}{\overline{\nu}_i}\sum_n eV_n\overline{\nu}_n}{e(V_A - V_C) + \frac{3}{2}kT_C - \frac{3}{2}kT_p} \quad ,$$

where V_i is the propellant ionization potential (for mercury V_i = 10.4 V), ν_i is the ionization frequency averaged over the electron energy distribution, ν_n is the averaged excitation frequency due to collisions of

atomic energy level n, V_n is the potential energy of level n, and k is the Boltzmann constant. The quantity η_m is the mass utilization efficiency and

$$\delta = \frac{\text{number of ionizations}}{\text{atom}} = \eta_m\left(\frac{2}{a} - 1\right),$$

where a is the transparency of the ion extraction system.

In practice, the measured value of source energy per ion V_S will exceed the minimum value to some extent as a result of less-than-optimum containment of primary electrons. Incomplete containment causes the average primary electron to arrive at the anode with an extra energy ΔE above the minimum possible average energy of $3/2\ kT_p$. The theory can be modified to include these additional losses by subtracting ΔE from the denominator in the expression for β and including it in the calculation of the term $1/\nu_i \sum_n eV_n \nu_n$ appearing in the numerator. Thus, for an LM cathode thruster which has not yet been optimized to the fullest extent, a new value β' can be written as

$$\beta' \equiv \frac{eV_i + e\Delta V_A + \frac{3}{2}kT_p + \frac{1}{\nu_i(\Delta E)}\sum_n eV_n \bar{\nu}_n(\Delta E)}{e(V_A - V_C) + \frac{3}{2}kT_C - \frac{3}{2}kT_p - \Delta E}$$

For an experimentally measured value of the source energy per ion V_S, eq. (1) can be modified as follows:

$$V_S = \frac{\beta'\delta}{\eta_m} V_A + \left(\frac{\delta}{\eta_m} - 1\right) V_A . \qquad (2)$$

Equation (2) is then used to evaluate the quantity β', from which the value of the quantity ΔE can be determined.

The distribution of heat inputs to the body of an LM cathode thruster can be evaluated in terms of the quantities defined above. The heat per beam ion which is lost to the cathode is given by

$$E_K = \frac{\beta' \delta}{\eta_m} V_{K,th}$$

where $V_{K,th}$ is the specific thermal loading of the cathode (see Section IV-B). The relationship for the heat per beam ion which is lost to the cathode cup is

$$E_C = \frac{\beta' \delta}{\eta_m} \left(V_C - \frac{3}{2} \frac{kT_C}{e} - V_{K,th} - \phi_K\right)$$

where V_C represents the total kinetic energy acquired by the electrons which accelerate from the cathode surface into the cathode-cup plasma. Of the three subtracted quantities, $3/2\ kT_C/e$ represents the average thermal energy carried away by electrons leaving the plasma of the cathode cup, $V_{K,th}$ represents the heating of the cathode itself, and ϕ_K is the work function potential which is required to liberate each electron from the liquid-mercury surface. Of the total kinetic energy, only the amount which remains after the three subtractions results in heating of the cathode cup.

Ions which reach thruster surfaces which are at cathode potential gain kinetic energy in falling through the potential drop. The heat per beam ion E_W which is lost to these walls is equal to the sum of the incident kinetic energy plus the difference between the energy of recombination V_i and the work function potential ϕ_K required to extract an electron from these surfaces.

$$E_W = \left(\frac{\delta}{\eta_m} - 1\right) \left((V_A + \Delta V_A) + (V_i - \phi_K)\right).$$

The heat per beam ion E_A which is carried to the anode by collected electrons is given by

$$E_A = \frac{\beta' \delta}{\eta_m} \frac{\Delta E}{e} + \left(\frac{\beta' \delta}{\eta_m} + \frac{\delta}{\eta_m} \right) \left(\frac{3}{2} \frac{kT_p}{e} + \phi_A \right).$$

The energy per beam ion E_ν which goes into excitation processes is given by the relationship

$$E_\nu = \frac{\delta}{n_m} E'_\nu$$

where

$$E'_\nu = \frac{1}{\bar{\nu}_i} \sum_n \bar{\nu}_n V_n.$$

(For the present analysis an approximate value $E'_\nu = 10$ eV is used.)

The inputs listed above represent thermal losses which are incurred in the process of generating the ion beam. The discharge power supply also provides the creation energy E_i for each ion entering the beam. This can be experessed as the potential energy of the ion relative to the potential of the anode electrode*

$$E_i = \Delta V + (V_i - \phi_A) \quad .$$

The sum of all the energy expenditures per beam ion which are listed above can be shown to be equal to the total source energy per beam ion V_S.

*For consistency in this analysis, the potential energy of both the beam ion and its associated secondary electron (generated as the other part of the ion pair) have been referenced to the Fermi level of the bound electrons within the anode material.

B. THERMAL ANALYSIS OF LMT-30-I

From experimentally measured operating parameters, the heat losses to an LM cathode thruster can now be determined. Using these as inputs to computer program TAS-1B, the temperature distribution for the LMT-30-I thruster is calculated below and compared with the measured distribution to demonstrate the efficacy of the analytical model.

Typical operating conditions for the LMT-30-I thruster are:

Beam current	I_B	= 1.09 A
Mercury flowrate equivalent	I_{Hg}	= 1.32 A
Discharge current	I_K	= 7 A
Discharge voltage	V_A	= 45 V
Source energy per ion	V_S	= 289 eV/ion
Mass utilization efficiency	η_m	= 82.5%
Special thermal load*	$V_{K,th}$	= 4 W/A.

Values for the electron temperatures and floating potentials of the discharge plasma are obtained from the results of Knauer, et al.[11] Although these data were generated with a hollow-cathode thruster, it is expected that they are more representative of the values to be found in the present LM cathode thrusters than are the existing data which were measured with an LM cathode thruster[3] prior to optimization of that thruster under the current contract. From the operating conditions listed above, values of the distribution of heat inputs to the LMT-30-I thruster are calculated as follows (refer to Fig. 22).

*The specific thermal load for the LM cathode $V_{K,th}$ is treated as a constant in the present calculations. For more precise results the dependence on temperature should be included and a self consistent solution must be found. The temperature dependence of the specific thermal loading $\left[V_{K,th}\,(T_K)\right]$ for LM cathode K-51 is given in Fig. 13, Section IV-B.

- Power to cathode, $P_K = I_K I_B = 24.2$ W
  (input to node 5)

- Power to cathode cup, $P_C = E_C I_B = 21.2$ W
  (half is assumed to be radiated to node 10 and the remaining half is radiated uniformly to all other nodes which are inside the discharge chamber)

- Power to cathode-potential walls, $P_W = E_W I_B = 51.1$ W
  (deposited uniformly in nodes 9, 10, 35, 42, and 49)

- Power to anode, $P_A = E_A I_B = 187$ W
  (67% of P_A is delivered to the front third of the anode, with the remainder distributed uniformly over the rest of the anode surface)*

- Power going into excitations, $P_\nu = E_\nu I_B = 21$ W
  (subsequently distributed uniformly as heat to all nodes which are inside the discharge chamber)

In addition, the following heat losses are included which are generated outside the discharge chamber:

- Power to the accel electrode, $P_{Ac} = 12.8$ W
  (delivered to nodes 41 and 48)

- Power dissipated in the magnets, $P_M = 12$ W
  (half goes into nodes 1, 2, and 3 and half into nodes 21, 23, 25, and 51)

The values of the radiation emissivities are representative of the surfaces of the various materials employed in fabricating the thruster.[12] Multiple heat shields are included in this analysis by the effective emissivity ϵ_e.

The emissivities, heat inputs, and resultant temperature profile for the LMT-30-I thruster are illustrated in Fig. 24. These results agree with a measured temperature profile which indicated that all external thruster surfaces operated at less than 200°C, except for the

*The total power to the anode was distributed in the manner which resulted in best agreement with experimental temperature measurements.

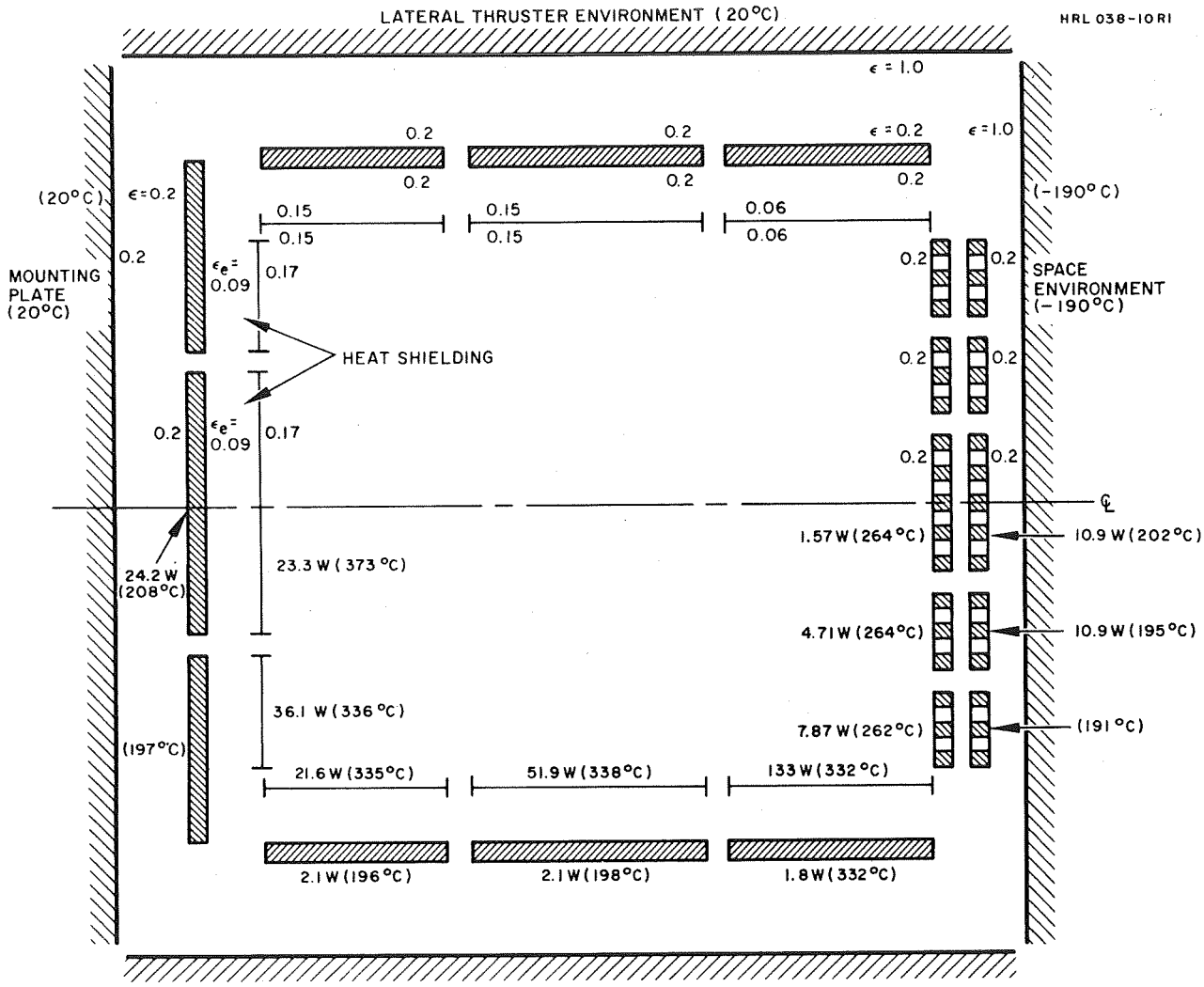

Fig. 24. Thermal model of the LMT-30-I thruster operating at a beam current I_B = 1.09 A. The emissivities and temperatures of fixed temperature walls are noted in the upper half of the schematic. The heat inputs and resultant temperature distribution are indicated in the lower portion of the diagram.

external anode connector which reached a temperature of 281°C. The thin stainless steel anode extension achieved a uniform temperature which was within 2°C of the downstream section of the anode. The good agreement between the experimental and analytical results with the LMT-30-I thruster indicates the usefulness of the analytical approach for thermal design of LM cathode thrusters in general.

C. THERMAL DESIGN OF LMT-20-II

Having been proven by experimental comparison with the LMT-30-I thruster, the technique for thermal analysis was employed in the design and analysis of the LMT-20-II thruster in an effort to predetermine its thermal operating characteristics. In addition to the study of the characteristics of a single thruster which radiates to space, emphasis has also been focused on the effect of assembling groups of thrusters in clustered arrays.

For these analyses, the operating conditions of the LMT-20-II thruster are taken to be:

- Beam current I_B = 1 A
- Mercury flowrate equivalent I_{Hg} = 1.18 A
- Discharge current I_K = 7 A
- Discharge voltage V_A = 40 V
- Source energy per ion V_S = 280 eV/ion
- Mass utilization efficiency η_m = 85%
- Specific thermal load $V_{K,th}$ = 4 W/A

As further input to the analysis, the outer surfaces of the LMT-20-II thruster body are taken to be covered with high emissivity (ϵ = 0.85) paint, and the values of the remaining emissivities are representative of the various materials employed in fabrication of the thruster.[12]

The emissivity of the upstream side of the thruster was set to zero (a perfect reflector) in order to represent thermal isolation of the feed system mounted adjacent to that surface. The analysis was based on the assumption of effective isolation of anode heat from the thruster shell by use of the 11 heat shields (consisting of 6061 aluminum foil), which cover both the inside surface of the thruster endplate and the upstream two-thirds of the anode.

The emissivities, heat inputs, temperatures of fixed-temperature walls, and resultant temperature profile are illustrated in Fig. 25 for a single thruster radiating to space. For this case the cathode attains a temperature of 121°C. This temperature is well within acceptable limits of operation of a single thruster and indicates a sufficiently high level of heat shield effectiveness to permit operation of multiple thrusters in clustered arrays with acceptable values of cathode temperature. (The characteristics of cluttered arrays are discussed in Section V-D).

D. ANALYSIS OF THERMAL CHARACTERISTICS

1. External Anode Connector

Until long-term effectiveness of multiple heat shielding has been demonstrated experimentally, a thruster configuration which employs an outer anode connector represents a conservative design approach. For moderately effective heat shielding, this configuration results in the lowest cathode temperature, and in all cases results in the lowest internal thruster temperatures. Furthermore, when an outer anode connector is employed, the cathode temperature is seen to be less sensitive to variation or deterioration in the effectiveness of multiple heat shielding.

If no outer anode connector is employed, analysis indicates that the interior of the discharge chamber attains a relatively high temperature (600° to 750°C) and the discharge heat is dissipated by radiation through the apertures of the ion-extraction system rather than from an

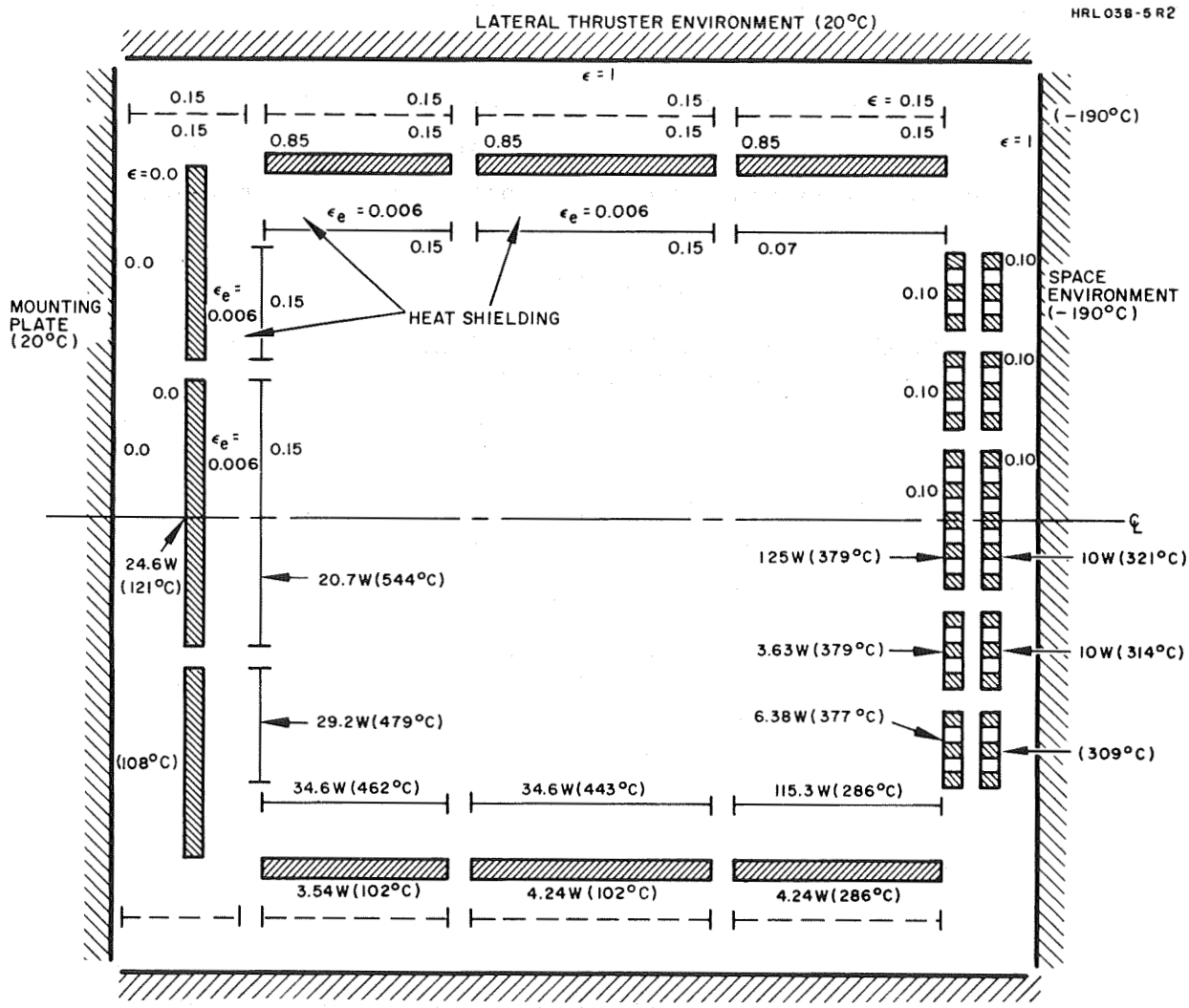

Fig. 25. Thermal model of the LMT-20-II thruster operating at a beam current I_B = 1 A. The emissivities and temperatures of the fixed-temperature walls are noted in the upper half of the schematic. The heat inputs and resultant temperature distribution are indicated in the lower portion of the diagram.

external anode connector. Table V compares the cathode temperature calculated both with and without an anode connector for two values of the effective emissivity ϵ_e, which is associated with multiple heat shields placed between the anode and the thruster shell. For the lower value of ϵ_e (a higher degree of insulation), the cathode temperature is lower for the geometry which does not employ an outer connector.

TABLE V

Effect of the Outer Anode Connector on Cathode Temperature T_K as a Function of the Effective Emissivity ϵ_e

Effective Emissivity ϵ_e	0.006	0.06
Cathode Temperature T_K (With Outer Anode Connector)	130°C	159°C
Cathode Temperature T_K (Without Outer Anode Connector)	80°C	173°C

The design value of the effective emissivity for the LMT-20-II thruster was calculated to be $\epsilon_e = 0.006$ by the assumptions that the surface of the heat shields retained the characteristic of clean aluminum $\epsilon_{Al} = 0.1$ and that conductive and convective heat transfer could be neglected. If this level of thermal isolation had actually been obtained, the outer anode connector would have ceased to serve a useful purpose and the cathode temperature would actually be increased by conduction or radiation from the outer connector to the thruster shell. The lower value $\epsilon_e = 0.06$ would correspond to the case that either heat transfer between adjacent heat shields did occur, or that the individual aluminum heat shields had lost their characteristic emissivity and approached a gray condition with $\epsilon = 0.5$. If the low values of the effective emissivity

cannot be maintained, the usefulness of the outer connector is apparent from the relative values of cathode temperatures which correspond to the higher value of effective emissivity. The actual experimental results represent a still worse case (corresponding to a value $\epsilon_e \approx 0.5$) in which the aluminum heat shields conduct freely to one another and that simultaneously the innermost shield (the stainless steel anode extension itself) has an emissivity of $\epsilon_e \approx 0.5$.

There is little doubt that techniques can be developed for more effective installation of heat shielding in the LM cathode thruster. The associated increase in the degree of thermal isolation between the anode and the thruster shell will result directly in a decrease of cathode temperature and above a certain level will provide the basis for a still more efficient design of an LM cathode thruster without an extended anode connector.

2. Clustered Arrays

The thermal characteristics of the design configuration of the LMT-20-II system (employing an outer anode connector and multiple heat shielding with an effective emissivity $\epsilon_e = 0.006$) have been analyzed to study the effects of combining many thrusters in a clustered planar array or in an infinite linear array. To the clustered planar array each thruster was assumed to be surrounded on all sides by a large number of identical thrusters, so that heat could be radiated only in the direction of the ion beam. The situation was analyzed by setting the emissivity of the lateral boundary of the thruster environment equal to zero (a reflecting boundary), in order to simulate the case of a central thruster surrounded by a set of identical thrusters which are separated by twice the distance of the reflecting boundary. The radius of this lateral boundary was varied between 1.5 and 3 times the thruster radius R in order to vary the view factor between the thruster side walls and the space environment. Figure 26 illustrates how the cathode temperature depends on the ratio of center-to-center separation to thruster

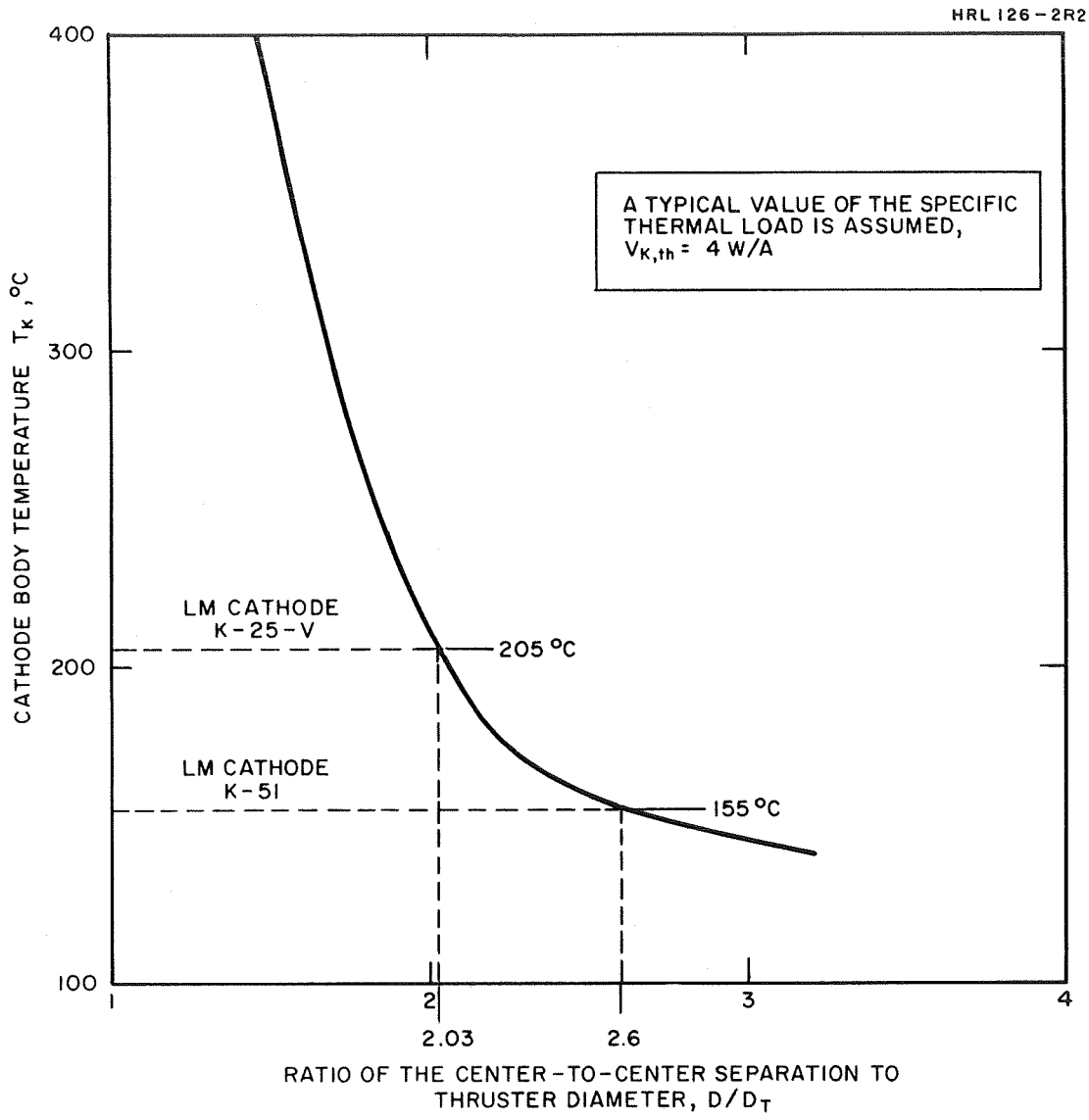

Fig. 26. Dependence of cathode temperature T_K on spacing between thrusters in an infinite array.

diameter D/D_T. At a beam current of 1 A, a self consistent solution for operation of the LMT-20-II thruster with LM cathode K-51 (i.e., $V_{K,th}$ = 4 W/A at T_K = 155°C) is achieved at a value D/D_T = 2.6. Closer spacings can be accommodated by use of an alternative LM cathode which exhibits a lower value of specific thermal loading at higher temperature. The specific thermal loading of LM cathode K-25-V, for example, reaches the value of specific thermal loading assumed for this analysis at a cathode body temperature T_K = 205°C. With this cathode, the required separation between thruster centers is reduced to 2.03 times the thruster diameter. For still closer spacings, additional means for heat dissipation are required. This can be provided by allowing heat conduction between the thruster and the spacecraft, or by using an additional radiator which can be connected to the thruster cathode by a heat pipe or other means. For the present configuration, no such mechanisms for heat transfer are included.

An infinite linear array of identical thrusters was analyzed for the case in which the thrusters are placed in contact with one another. To simulate this configuration without introducing the complexity of azimuthal asymmetry, a model is used in which the lateral environment of an individual thruster is made to be uniform with an emissivity which is the average of the emissivities appropriate for a thruster in a linear array. An average emissivity of 0.67 is obtained by using the simplifying approximation that each incremental area on the lateral thruster surface radiates only in the radial direction. In this case, two-thirds of the lateral thruster surface radiates to space, which has unity emissivity, and one-third of the surface radiates to an identical operating thruster which can be represented by a surface with an emissivity of zero. For these parameters, the computer-simulated thermal model predicts a cathode temperature of 164°C. This is within the desirable operating temperature range of the LM cathode thruster, and thus the feasibility of operation in a close-packed linear array is established.

SECTION VI

CONCLUSIONS

Efficient performance has been demonstrated in operation of a flight-type 20 cm electron-bombardment mercury ion thruster utilizing a liquid metal (LM) cathode which is thermally integrated with the aluminum body of the thrust chamber. The thruster system, designated LMT-20-II, operates over a design range of beam current from I_B = 0.5 A to 1.0 A at a nominal beam voltage V_B = 2 kV. At full beam power, the cathode temperature is held at a value T_K = 200°C by a balance between discharge heating and cooling by radiation from the outer walls of the thrust chamber. Discharge chamber performance is essentially unchanged for operation at an effective specific impulse $I_{sp,eff}$ = 2710 sec. The LMT-20-II system includes a liquid mercury feed system with the capability for automatic flow control and high voltage isolation between the thrust chamber and the propellant reservoir. Over-all system efficiency is comparable to that of other electron bombardment thruster types.

Specific accomplishments under the current phase of this contract include the following.

1. The experimental LMT-20-I thruster was optimized for operation at a beam voltage V_B = 2 kV in order to predetermine optimization modifications for the LMT-20-II thruster. The best performance was achieved at a beam current I_B = 950 mA with a total source energy per ion V_S = 383 eV/ion* and a mass utilization efficiency η_m = 88%.

2. The LMT-20-II, including the mercury feed subassembly, has been operated over its design range from I_B = 0.5 A to 1.0 A with an over-all efficiency η_T = 72% for operation

*V_S, the total source energy per ion, is the discharge energy per ion because no heater, vaporizer, or keeper power is required with the LM cathode.

at the design impulse $I_{sp,eff}$ = 4,040 sec. Operation has also been demonstrated with an over-all efficiency η_T = 60% at $I_{sp,eff}$ = 2710 sec.

3. A prototype model of a liquid mercury flowmeter has been tested which shows promise of a measurement accuracy of ±1%. The flowmeter operates with a power expenditure of 1 W.

4. An electromagnetic pump using molybdenum electrodes has been operated for over 800 hours at a pressure rise of 0.6 atm with a power expenditure of 2 W.

5. A high voltage isolator has been developed and has been operated reliably and repeatedly for over 500 hours. The average power expenditure is 0.7 W when operated in the pulsed-only heating mode.

6. An all solid-state power conditioner subsystem has been completed which contains the electronic circuitry necessary to provide appropriate power inputs (from a solar array power source) for the EM pump and the high voltage isolator of the LMT-20-II feed system.

7. The thermal profile of the LMT-30-I thruster was calculated by analytical techniques and shown to agree with the experimentally measured profile. This correspondence confirms the validity of the analytical approach.

8. A program of thermal analysis has been completed in which the thermal properties of the LMT-20-II thruster were determined using the same analytic techniques that were verified experimentally with the LMT-30-I thruster. The analysis indicates that when effective heat shielding is employed between the anode extension and the thruster shell, the temperature of the LMT-20-II thruster will remain within acceptable limits when operated within the design current range. No constraint is imposed by arranging groups of thrusters in a closely packed linear array. Groups of thrusters operated in infinite planar clusters will achieve satisfactory thermal balance by selfradiation alone, so long as the separation between thrusters is equal to at least twice the thruster diameter.

SECTION VII

RECOMMENDATIONS AND FUTURE PLANS

1. It is apparent from thermal analysis that significant reduction of cathode temperature can be achieved by use of even moderately effective heat shielding between the anode and thruster shell. This reduction should be demonstrated experimentally to exhibit the capability for system operation in clustered arrays and to examine the feasibility of an even more efficient thermal design which does not employ an external anode connector.

2. More extensive and exhaustive optimization of discharge chamber performance should be carried out. Because of the limited opportunity under the subject contract for changes in the discharge-chamber configuration of the LMT-20-II system, sizable reductions in source energy per ion can be expected. While such reductions are of benefit in their own right, the decrease in discharge chamber losses will extend the thermal range for operation of the LMT-20-II system.

3. The LMT-20-II system should be extended to include a flight-type LM cathode discharge igniter and LM cathode neutralizer to permit meaningful evaluation of a complete thruster system with respect to other thruster types.

4. While a basic capability for throttling over a 2:1 range in beam current has been demonstrated by the data of Fig. 4, the separate performance data curves were individually optimized by means of small variations in magnetic field intensity and baffle position. A true throttling characteristic (such as the throttling data for the LMT-20-I thruster presented in Fig. 6 of Ref. 1) should hold fixed the baffle position if not also the magnetic field intensity. Under these conditions, throttling characteristics similar to those demonstrated for the LMT-20-I thruster are anticipated for the LMT-20-II system.

5. Implementation of a variable magnetic baffle configuration[13] is recommended for extending the throttling limits of the LMT-20-II system, while maintaining optimum performance throughout these limits.

6. Development of flight-type supplemental power-conditioning circuitry for the LMT-20-II system is recommended as a prelude to meshing the supplemental circuitry with the power-conditioning circuitry used in common with the JPL SEPST III system.

7. An LM cathode should be developed which combines the best features of LM cathode K-25-V (low $V_{K,th}$ at high operating temperature) with the flight-type design of LM cathode K-54.

8. Development of small (5 cm anode diameter) LM cathode thrusters would demonstrate a unique capability of the LM cathode thruster system for efficient operation in the low current range, because the LM cathode needs no vaporizer or cathode heater for its operation. In this range of thruster size, the auxiliary heater power represents a major fraction of the total power consumption.

9. The LM cathode thruster should be equipped with dielectric coated grids if they continue to show promise for use in ion propulsion systems. This conversion is expected to result in more efficient discharge chamber performance at very low values of specific impulse.

SECTION VIII

NEW TECHNOLOGY

A. FIRST QUARTER

During the first quarter of the current phase of this contract, an invention which is believed to be patentable was reduced to practice. Accordingly, the following patent disclosure was submitted to the Patent Department of the Hughes Aircraft Company.

PD 69419, Sensitive Liquid-Metal Flow Meter, by Julius Hyman, Jr.

The principles upon which this invention is based are reported to NASA on pp. 21-23 of the First Quarterly Report, 15 May 1968, covering Phase I of this contract. Further details concerning the operation of this device are contained on pp. 35-37 and in the Appendix of Quarterly Progress Report No. 1, 15 October 1969, covering Phase II of this contract.

B. SECOND QUARTER

No reportable items of new technology were identified during the second quarter of the subject effort.

C. THIRD QUARTER

No reportable items of new technology were identified during the third quarter of the subject effort.

D. FOURTH QUARTER

No reportable items of new technology were identified during the fourth quarter of the subject effort.

REFERENCES

1. J. Hyman, Jr., W.O. Eckhardt, J.R. Bayless, J.A. Snyder, and J.W. Pfeifer, "High Temperature LM Cathode Ion Thrusters." Final Report, Contract JPL 952131, 1969, Hughes Research Laboratories, Malibu, California.

2. T.D. Masek and E.V. Pawlik, "Thrust System Technology for Solar Electric Propulsion," Paper No. AIAA 68-541, 4th Propulsion Joint Specialists Conference, Cleveland, Ohio, June 1968.

3. W.O. Eckhardt, K.W. Arnold, G. Hagen, J. Hyman, Jr., J.A. Snyder, and R.C. Knechtli, "High Temperature Liquid Mercury Cathodes for Ion Thrusters," Summary Report Contract NASW-1404, July 1967, Hughes Research Laboratories, Malibu, California.

4. W.O. Eckhardt, H.J. King, J.A. Snyder, J.W. Ward, G. Hagen, W.D. Myers, and R.C. Knechtli, "Liquid Mercury Cathode Electron-Bombardment Ion Thrusters," Summary Report, Contract NAS 3-6262, October 1966, Hughes Research Laboratories, Malibu, California.

5. J.H. Molitor, H.J. King, and S. Kami, "A Study of Liquid Mercury Isolator Development," Contract NAS 7-539, September 1967, Hughes Research Laboratories, Malibu, California.

6. R.T. Bechtel, "Discharge Chamber Optimization of the SERT II Thruster," AIAA Paper No. 67-668.

7. Liquid Metals Handbook, U.S. Government Printing Office, 2nd Ed., 165, (June 1954). J. Nejedlik and E. Vargo, "Material Resistance to Mercury Corrosion," Electrochemical Technology, 3, 9-10, 250 (1965). W. Latimer and J. Hildebrand, Principles of Chemistry and Reference Book of Inorganic Chemistry (Macmillan, New York, 1940), 90. H. Logan, The Stress Corrosion

of Metals (Wiley, New York, 1966), 193. H. Uhlig, The Corrosion Handbook (Wiley, New York, 1948), 618. B. Power and F. Robson, "Experiences with Demountable U.H.V. Systems," Tech. Rep. of Edwards High Vacuum Ltd., Crawley, Sussex, England.

8. J. Hyman, Jr., J.R. Bayless, D.E. Schnelker, J.W. Ward, and R.L. Seliger, "LM Cathode Thruster System," Quarterly Progress Report No. 1, Phase II, Contract JPL 952131, October 1969, Hughes Research Laboratories, Malibu, California.

9. W. Knauer, "Power Efficiency Limits of Kaufman Thruster Discharges," AIAA Paper No. 70-177, AIAA 8th Aerospace Sciences Meeting, January 19-21, 1970, New York, New York.

10. "Ion Engine Thrust Vector Study," Final Report, Contract JPL 952129, 1968, Hughes Research Laboratories, Malibu, California.

11. W. Knauer, R.L. Poeschel, H.J. King, and J.W. Ward, "Discharge Chamber Studies for Mercury Bombardment Ion Thrusters," Final Report, Contract NAS 3-9703, September 1968.

12. W.L. Wolfe, Handbook of Military Infrared Technology, Office of Naval Research, Washington, D. C. 1965.

13. R.L. Poeschel and W. Knauer, "A Variable Magnetic Baffle for Hollow Cathode Thrusters," Research Report No. 417, December 1969, Hughes Research Laboratories, Malibu, California.